

6 Planetary Magnetospheres

Fran Bagenal

Astrophysical and Planetary Sciences, Dept. and Laboratory for
Atmospheric and Space Physics, University of Colorado, Boulder,
CO, USA

1	<i>Introduction</i>	252
2	<i>Magnetospheric Principles</i>	254
2.1	Planetary Magnetic Fields	254
2.2	Scales of Planetary Magnetospheres	260
2.3	Plasma Sources	263
2.4	Plasma Dynamics	266
2.4.1	Energetic Particles and Radiation Belts	267
2.4.2	Rotational Flows	271
2.4.3	Global Solar-Wind-Driven Convection	273
2.4.4	Plasmoid Ejection	277
3	<i>Magnetospheres of the Outer Planets</i>	278
3.1	Jupiter	279
3.2	Saturn	285
3.3	Uranus and Neptune	290
4	<i>Small Magnetospheres</i>	292
4.1	Mercury	293
4.2	Ganymede	293
5	<i>Induced Magnetospheres</i>	295
5.1	Venus	295
5.2	Mars	297
5.3	Titan	298
5.4	Io	298
5.5	Pluto and Comets	302
6	<i>Outstanding Questions</i>	302
	<i>References</i>	303

Abstract: The nature of interaction between a planetary object and the surrounding plasma depends on the properties of both the object and the plasma flow in which it is embedded. A planet with a significant internal magnetic field forms a magnetosphere that extends the planet's influence beyond its surface or cloud tops. There are seven objects in the solar system that presently have internally generated magnetic fields: Mercury, Earth, Jupiter, Saturn, Uranus, Neptune, and the satellite Ganymede. A planetary object without a significant internal dynamo can interact with any plasma flowing past via remanent magnetization of the crust and/or currents associated with local ionization or induced in an electrically conducting ionosphere or layer of water. Venus, Mars, Titan, Io, Enceladus, and Europa have strong interactions with their surroundings. Planetary magnetospheres span a wide range of sizes but involve similar basic principles and processes.

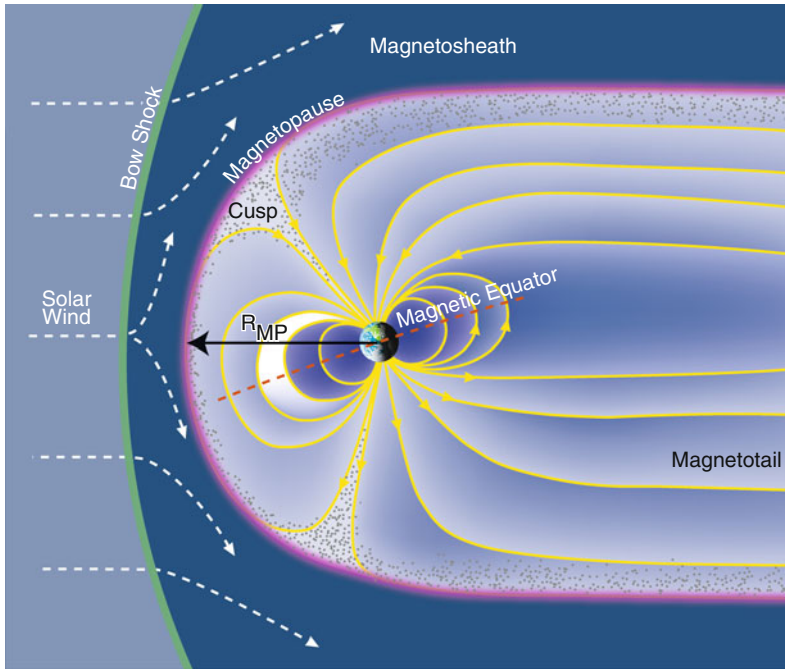
Keywords: Aurora; Bow shock; Compression; Conductivity; Convection; Corotation; Diffusion; Dipole; Dynamo; Flux rope; Instability; Interchange; Io Plasma torus; Ion escape; Ionosphere; Kelvin–Helmholtz; Magnetic moment; Magnetization; Magnetopause; Magnetosheath; Magnetosphere; Magnetotail; Multipole; Non-dipole magnetic fields; Plasma sources; Plasma-pause; Plasmasphere; Plasmoids; Radiation belts; Radio emission; Reconnection; Remanent magnetization; Rotation; Solar wind; Sputtering; Stagnation

1 Introduction

As the name suggests, a planet's *magnetosphere* is the region of space influenced by the planet's magnetic field. The nature of the interaction between a planetary object and the surrounding plasma depends on the properties of both the object and the plasma flow in which it is embedded. A planet with a significant internal magnetic field forms a magnetosphere that extends the planet's influence beyond its surface or cloud tops. A planetary object without a significant internal dynamo can interact with any surrounding plasma via remanent magnetization of the crust and/or currents induced in an electrically conducting ionosphere or layer of water.  [▶ Figure 6-1](#) is a schematic of the archetypical magnetosphere of Earth, illustrating the general anatomy.

All solar system objects are embedded in the *solar wind* that streams radially away from the Sun. The flow speed of the solar wind exceeds the speed of the fastest wave mode that can propagate in the interplanetary plasma. The interaction of the supersonic solar wind with a planetary magnetic field (either generated by an internal dynamo or induced externally) produces a *bow shock* upstream of the planet. Behind the bow shock, the subsonic wind – the *magnetosheath* – is deflected around the magnetospheric obstacle. The magnetospheric boundary – the *magnetopause* – was usually regarded to first order as an impenetrable boundary. However, the amount of mass, momentum, and magnetic flux exchanged across the magnetopause has become an active area of research at Earth and other magnetospheres. The distance between the center of the planet and the magnetopause in the direction of the Sun (approximately the closest distance) is labeled R_{MP} , generally described in units of the planetary radius (R_P). Whatever the details of the interaction, in nearly all cases, the interaction region has a “wake” or “tail” – the *magnetotail* – that can extend for several hundred times R_{MP} downstream in the solar wind.

Venus, Mars, and (likely) Pluto do not have dynamos generating an internal field at present, though strong remanent magnetization of crustal rocks is evidence that Mars certainly had a dynamo in the past and this is also quite possible for Venus too. At present, the solar wind



■ Fig. 6-1
Anatomy of a magnetosphere, applied here to Earth

interacts with the substantial ionospheres of these planets, induction currents deflecting the bulk of the flow around the planet, acting as the obstacle to the supersonic solar wind, and producing an upstream bow shock. Any neutral atoms or molecules escaping from planetary atmospheres often become ionized either by solar photons or charge exchange with solar wind protons. These atmospheric ions are then entrained in and extract momentum from the solar wind. The slowing of the solar wind around these obstacles carries the Sun's magnetic field which is then temporarily draped around the planet and stretched back into a comet-like tail.

Objects such as the Earth's Moon that have no appreciable atmosphere and a low-conductivity surface have minimal electrodynamic interaction with the surrounding plasma and just absorb the impinging solar wind with no upstream shock. Interactions between planetary satellites and magnetospheric plasmas are as varied as the moons themselves: Ganymede's significant dynamo produces a mini-magnetosphere within the giant magnetosphere of Jupiter; the electrodynamic interactions of magnetospheric plasma flowing past volcanically active Io (Jupiter) and Enceladus (Saturn) generate substantial currents and supply extended clouds of neutrals that become ionized to supply more plasma to the system; plasma interactions with Titan's thick atmosphere and substantial ionosphere are likened to Venus; in the absence of an atmosphere, charged particles bombard the moon surfaces, sometimes sputtering significant exospheres (e.g., Europa, Dione, Callisto). The flow within magnetospheres tends to be subsonic, so that none of these varied interactions forms a shock upstream of the moon.

Reviews of planetary magnetospheres range in their approach to the subject from considering it a topic in space plasma physics (exploiting the range of planetary environments as a laboratory to explore space plasmas) to a branch of planetary science (presenting the space

environment as a component in understanding the planetary objects). A basic, qualitative introduction is given in van Allen and Bagenal (1999). Deeper studies of comparative magnetospheres range from the abstract to the specific (Siscoe 1979; Vasyliūnas 2004; Vasyliūnas 2009, 2010; Kivelson 2007; Walker and Russell 1995; Bagenal 1992; Russell 2004, 2006; Kivelson and Bagenal 2007; Bagenal 2009). This chapter takes an intermediate path, with the goal of applying the general principles to specific planets but also providing a qualitative appreciation of the different characters of our local family of magnetospheres.

The general principles of the structure and dynamics of planetary magnetospheres are presented in [Sect. 2](#). The Earth is the nominal case with which to compare the basic properties between the planets. [Section 3](#) introduces the magnetospheres of the outer planets, magnetospheres that are large, dominated by rotation, and strongly influenced by the moons that are embedded within. By contrast, [Sect. 4](#) discusses the mini-magnetospheres of Mercury and Ganymede. [Section 5](#) returns to plasma interactions with nonmagnetized objects where the varied plasma interactions with planets such as Venus, Mars, and Pluto are discussed, as well as moons Titan, Io, Enceladus, and Europa.

2 Magnetospheric Principles

The interaction of a planetary object with its surroundings depends on the properties of both the planetary body and the impinging plasma. For the nine major planetary bodies, [Table 6-1](#) lists the properties of the interplanetary medium (the strength and direction of the interplanetary magnetic field (IMF) and the speed, density, and temperature of the solar wind), as well as the strength of any planetary magnetic field, the planetary rotation rate, and the scale of the observed magnetospheres. In [Table 6-2](#), the properties of the planetary dynamos are listed: the strength and direction of the planet's magnetic field and the direction of the planet's spin. Below, how these properties affect the characteristics and behavior of planetary magnetospheres is discussed.

2.1 Planetary Magnetic Fields

Spacecraft carrying magnetometers have flown to and characterized the magnetic fields of all the planets except (dwarf) Pluto. All four of the giant planets have strong magnetic fields. The smaller terrestrial planets have weaker fields, Mercury's being much weaker than Earth's. The upper limit on an internally-generated field of Venus is less than 10^{-5} times Earth's magnetic moment. While strong magnetization of surface rocks show that Mars' internal dynamo was active in the past, geological evidence shows that the dynamo shut down around 4 billion years ago.

The history of space exploration of planetary magnetism is given by Ness (2010), while Balogh (2010) reviews techniques that have been employed to measure planetary magnetic fields. Thorough reviews of planetary magnetic field observations and their analysis are presented for all planets by Connerney (2007) and for the giant planets by Russell and Dougherty (2010). Anderson et al. (2010, 2011) present recent determinations of Mercury's magnetic field from the MESSENGER spacecraft. Magnetic field measurements from orbit allow the separation of the internally generated field from the effects of external currents in the magnetosphere (see review by Olsen et al. 2010 of the techniques for doing this).

Table 6-1
Properties of the solar wind and scales of planetary magnetospheres

	Mercury	Venus	Earth	Mars	Jupiter	Saturn	Uranus	Neptune	Pluto
Distance from Sun, a_p (AU) ^a	0.39	0.72	1 ^b	1.52	5.2	9.5	19	30	40
Solar wind density ^b (cm^{-3})	53	14	7	3	0.2	0.07	0.02	0.006	0.003
IMF strength ^c (nT)	41	14	8	5	1	0.6	0.3	0.2	0.1
IMF azimuth angle ^c	23°	38°	45°	57°	80°	84°	87°	88°	88°
Radius, R_p (km)	2,440	6,051	6,373	3,394	71,400	60,268	25,600	24,765	1,170 (± 33)
Sidereal spin period (day)	58.6	-243	0.9973	1.026	0.41	0.44	-0.72	0.67	-6.39
Magnetic moment ^d (M_E)	$3-6 \times 10^{-4}$	$<10^{-5}$	1	$<10^{-5}$	20,000	600	50	25	?
Surface magnetic field ^e B_0 (nT)	195	-	30,600	-	430,000	21,400	22,800	14,200	?
R_{CF} (R_p)	1.6 R_M	-	10 R_E	-	46 R_J	20 R_S	25 R_U	24 R_N	?
Observed R_{MP} (R_p)	1.5 R_M	-	8-12 R_E	-	63-92 R_J	22-27 R_S	18 R_U	23-26 R_N	?

^aSemimajor axis of orbit. 1 AU = 1.5×10^8 km

^bThe number density of the solar wind fluctuates by about a factor of 5 about typical values of $n_{sw} \sim 7 \text{ (cm}^{-3}\text{)}/a_p^2$. The mass density of the solar wind is $\rho_{sw} = 1.04 n_{sw} \text{ (amu cm}^{-3}\text{)}$

^cMean values for the interplanetary magnetic field (IMF) in units of nano-Tesla with spherical components B_r, B_θ, B_ϕ . The azimuth angle is $\tan^{-1}(B_\phi/B_r)$. The radial component of the IMF, B_r , decreases as $1/a_p^2$, while the transverse component, B_ϕ , increases with distance

^d $M_{Earth} = 7.9 \times 10^{25} \text{ G cm}^3 = 7.9 \times 10^{15} \text{ T m}^3$

^eMagnitude of dipole (see text for references)

^f R_{CF} is calculated using $R_{CF} = \xi (B_0^2/2\mu_0\rho V_{sw})^{2/6}$ for typical solar wind conditions of ρ_{sw} given above and $V_{sw} \sim 400 \text{ km s}^{-1}$ and ξ an empirical factor of ~ 1.4 to match Earth observations (Walker and Russell 1995)

■ **Table 6-2**
Planetary magnetic fields

	Ganymede	Mercury	Earth	Jupiter	Saturn	Uranus	Neptune
B_{dipole}^a (nT)	719	195	30,600	430,000	21,400	22,800	14,200
Maximum/minimum ^b	2	~2	2.8	4.5	4.6	12	9
Dipole tilt and sense ^c	-4°	<+3°	+9.92°	-9.4°	-0.0°	-59°	-47°
Dipole offset ^d (R_p)		~0.2	-	0.119	0.038	0.352	0.485
Obliquity ^e	0°	0°	23.5°	3.1°	26.7°	97.9°	29.6°
Range in solar wind angle ^f	90°	90°	67 – 114°	87 – 93°	64 – 117°	8 – 172°	60 – 120°

^aSurface field at dipole equator. Values derived from modeling the magnetic field as an offset, tilted dipole (OTD)

^bRatio of maximum surface field to minimum (equal to 2 for a centered dipole field). This ratio increases with larger non-dipolar components and tends to increase with the planet's oblateness

^cAngle between the magnetic and rotation axes. Positive values correspond to magnetic field directed north at the equator

^dValues for the giant planets come from dipole (OTD) models of Connerney (1993, 2007). The Earth's dipole is from the International Geomagnetic Reference Field, while the magnetic dip poles of the Earth's field are located (in 2010) at 85° N and 64° S latitudes and moving over 10° per century (Finlay et al. 2010). Mercury's magnetic field is from Anderson et al. (2011)

^eThe inclination of a planet's spin equator to the ecliptic plane

^fRange of angle between the radial direction from the Sun and the planet's rotation axis over an orbital period. In Ganymede's case, the angle is between the corotational flow and the moon's spin axis

As planetary magnetic field measurements are improved (in coverage, accuracy, and proximity to the planet), they tend to show increasing complexity. The standard technique is to describe the internal magnetic field as a sum of multipoles or spherical harmonics (e.g., Walker and Russell 1995; Connerney 1993, 2007; Merrill et al. 1996), the higher orders being functions that drop off increasingly rapidly with distance so that one needs to get very close to the planet to see any effects of these high-order multipoles. The amplitude of each multipole is derived by fitting magnetic field observations obtained by magnetometers on spacecraft flying past the planet (e.g., Connerney 1981; Russell and Dougherty 2010). The extensive coverage provided by surface explorers over the centuries and afforded by low-orbiting spacecraft at Earth in the past 50 years not only allows the present Earth's field to be described with hundreds of terms but also allows description of the variation of the Earth's field over time (e.g., reviewed by Hulot et al. 2010). Moreover, paleomagnetic data extend the Earth's record back in geological time, revealing many polarity reversals of the magnetic field. By contrast, the sampling of planetary magnetic fields is too poor to determine any temporal variation over the few decades of space exploration, and currently there is no evidence of whether other planetary dynamos reverse polarity.

For magnetospheric purposes, where one is relatively far from the planet, a simple dipole description (equivalent to a bar magnetic placed inside the planet) has proved to be very valuable. The formula for a dipole magnetic field vector (measured in units of Tesla) \mathbf{B} as a function of position vector \mathbf{r} is

$$B = [3r(M \cdot r) - Mr^2]/r^5, \quad (6.1)$$

where M is the planetary magnetic moment (in units of T m^3). It is easier to understand this vector field if one looks at the components (B_r, B_θ, B_ϕ) in a spherical coordinate system (r, θ, ϕ), centered and aligned with the dipole. For a dipole centered on the planet, the field is azimuthally symmetric and $B_\phi = 0$, while the other components are

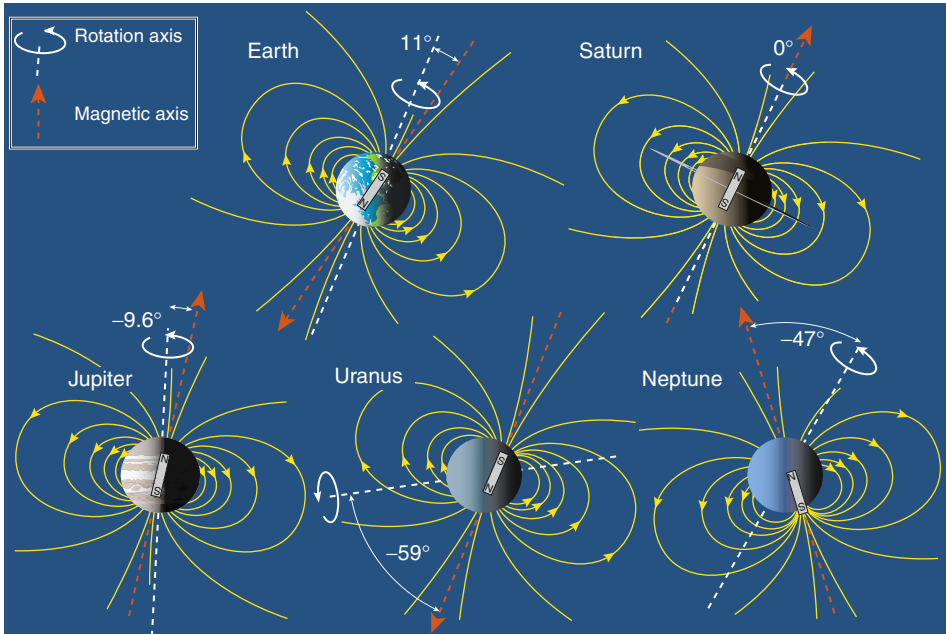
$$B_r = 2B_o \cos \theta / R^3 \quad (6.2)$$

$$B_\theta = B_o \sin \theta / R^3 \quad (6.3)$$

$$|B| = B_o (1 + 3 \cos^2 \theta)^{1/2} / R^3. \quad (6.4)$$

where B_o is the value of the magnetic field at the equator, $R = |r|/R_p$, and θ is colatitude. Note that the field strength at the poles ($\theta = 0$) is twice that at the equator, B_o .

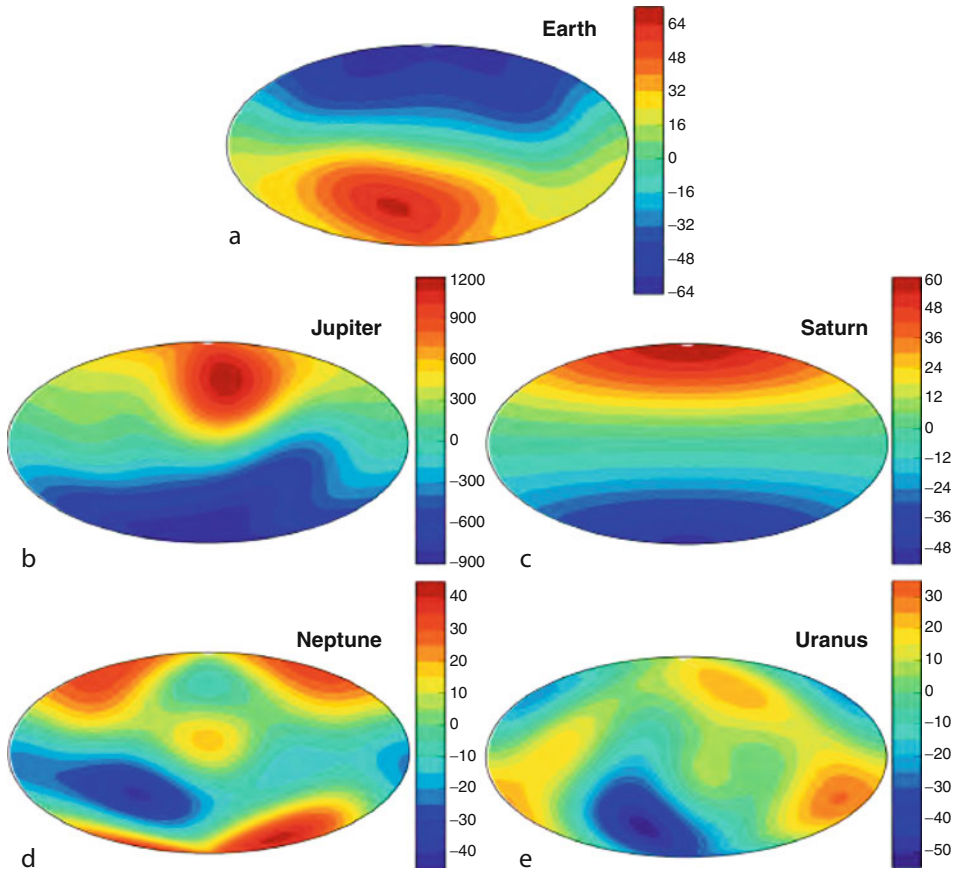
The planetary magnetic fields are generally not aligned with the planet's spin axis. Thus, the simplest description is often a dipole that is offset from the center of the planet and tilted. **Figure 6-2** illustrates the offset, tilted dipole (OTD) that approximates planetary fields and the values are given in **Table 6-2**. Except for Uranus and Neptune, the tilts are modest ($<10^\circ$) and the offset a small fraction of a planetary radius. The large tilts and offsets of Uranus' and Neptune's magnetic fields indicate the highly non-dipolar nature of these fields. Further indication of deviation of the true magnetic field from the simplicity of centered dipole is illustrated by the ratio of maximum to minimum surface field strength being much larger than value of 2 expected for a centered dipole. The range of complexities from Saturn's highly symmetric, dipolar field to the irregular fields of Uranus and Neptune are illustrated in the surface maps of magnetic field strength shown in **Fig. 6-3** and the high values of the max/min ratio in **Table 6-2**.



■ Fig. 6-2

The tilt angles between the spin and magnetic axes are shown for the five main magnetized planets. Considering the horizontal direction of the diagram to be parallel to the ecliptic plane and the vertical direction the ecliptic normal, then the spin axis is shown for conditions of maximum angle from the ecliptic normal (i.e., at solstice). Each planet's magnetic field can be approximated as a dipole where the orientation and any offset from the center of the planet is illustrated by a bar magnet located at the center of the planet

While the theory of planetary dynamos has yet to reach the level of sophistication where it could predict with accuracy the presence (let alone the specific characteristics) of an internally generated magnetic field, it is generally understood that, for such a field to be present, planets need to have an interior that is sufficiently electrically conducting and that is convecting with sufficient vigor. Various simple scaling laws have been derived over the years (e.g., reviewed by Christensen 2010) that relate the strength of the planet's magnetic field to other properties, but these laws seem to be more useful for testing theoretical ideas about dynamos than for predictions. Extensive geophysical measurements have revealed substantial information about the distribution of density, temperature, and flows inside the Earth. Moreover, the remanent magnetization of surface rocks tells us how the Earth's field has changed over geological time. These geophysical data are powerful constraints on the geodynamo and numerical dynamo models are beginning to show consistent behavior (Christensen 2010; Wicht and Tilgner 2010). In addition, laboratory experiments test ideas about parameters that control geodynamo behavior (Verhille et al. 2010). For other planetary objects, where information about the interior properties is much more limited, the presence or absence of a magnetic field is an important constraint on the interior conditions. Dynamo models are now being developed that vary the size of the planetary core, rotation rate, conductivity, heat flux, etc., to match the wide range of conditions at different planets (reviewed by Stanley and Glatzmaier 2010).



■ Fig. 6-3

Surface maps of the strength of the radial component of magnetic field for (a) Earth, (b) Jupiter, (c) Saturn, (d) Neptune, and (e) Uranus. For the gaseous planets, the surface is taken to mean the 1 bar pressure level (Data from Merrill et al. (1996) for Earth, Connerney (1993) for Jupiter and Saturn and Holme and Bloxham (1996) for Uranus and Neptune. Based on Stanley and Bloxham (2006))

Given the disparity in scale between the giant and terrestrial planets (e.g., the volume of Jupiter is 1,400 times that of the Earth), it is perhaps not surprising that the four terrestrial planets have far weaker magnetic fields generated in their interiors than the giant planets (Russell 1993; Connerney 1993; Stevenson 2003; Breuer et al. 2010). The iron cores are potential dynamo regions of terrestrial planets. The high pressures inside the giant planets Jupiter and Saturn put the hydrogen into a phase where it has the electrical conductivity of liquid metal (see ► Chap. 4). Jupiter's three times higher mass than Saturn produces a much larger volume of metallic hydrogen, responsible for ~ 20 times stronger dynamo. Inside Uranus and Neptune, the pressures are too weak to make hydrogen metallic, and it is postulated that their dynamos must be generated in regions of liquid water where, as in Earth's ocean, small concentrations of ions provide sufficient conductivity. Stanley and Bloxham (2006) show that confining the dynamos of these water giants to a relatively thin conducting shell can produce highly irregular, non-dipolar magnetic fields.

Careful analysis by Phillips and Russell (1987) produced an upper limit to Venus' magnetic moment of $\sim 1 \times 10^{-5} M_E$ and revealed no evidence of crustal remanent magnetization. The apparent lack of an active dynamo inside Venus puts interesting constraints on the thermal evolution of that planet (Stevenson et al. 1983; Schubert et al. 1988). A common misconception is that it is the slowness of the rotation of Venus that prevents a dynamo. In fact, very little rotation is needed for a dynamo, and all objects in the solar system have sufficient rotation (Stevenson 2003). So, the question becomes why is Venus' core not convecting? Stevenson et al. (1983) proposed that Venus' core temperature is too high for a solid iron inner core to condense (the differentiation of solid iron from an outer liquid sulfur-iron alloy drives Earth's dynamo). The lack of plate tectonics at Venus may be limiting the cooling of the planet's upper layers, further suppressing internal convection. Another possibility is that Venus may be in a state of transition following the period of global volcanism that resurfaced the planet about 700 million years ago (see ► Chap. 3). Thus, Venus might have had an active dynamo in the past and may well develop one in the future. Why neighbor twin planets should have suffered such different internal histories is a major mystery of planetary geophysics (Smrekar et al. 2007).

Measurements of strong remanent crustal magnetism (surface fields of up to 1,500 nT) suggest that Mars has had an active dynamo and experienced changes in polarity over geological time scales (Acuña et al. 2001; Connerney et al. 2004) but stopped generating an internal field some 4 billion years ago. Stevenson (2010) summarizes the three main contending theories of how Mars' dynamo operated for a few hundred million years and then ceased: (1) cooling of the core slowed down to the point where conductive heat loss dominated, without an inner core forming (Stevenson et al. 1983); (2) Nimmo and Stevenson (2000) suggest that after a period of efficient convection (perhaps driven by plate tectonics), Mars underwent a change in convective style to the currently observed stagnant lid mode, causing the mantle and core to stop cooling and turning off core convection and the dynamo (note that this model would work irrespective of whether Mars has an inner core); or (3) the inner core of Mars froze sufficiently so that the remaining fluid region of the outer core was too thin to sustain a dynamo (Stewart et al. 2007). These theories span a wide range of states of the core of Mars. Future geophysical sounding (in particular, seismology) will hopefully reveal the state of Mars' interior.

Having radii of ~40% of the Earth's radius, Mercury and Ganymede were originally expected to have cooled off, shutting down any internal dynamo. But spacecraft flybys showed each object to have a significant magnetic field. Thermal models of the particularly large iron core (>70% of the radius) of Mercury suggest that at least an outer region is likely to be liquid and possibly convecting. However, the observed field is much weaker than standard dynamo theory would predict (Stevenson 2003). Efforts to reconcile models of thermal evolution (Breuer et al. 2010) and dynamo models (Stanley and Glatzmaier 2010) of these small bodies is an active area of research.

2.2 Scales of Planetary Magnetospheres

The term "magnetosphere" was coined by Gold (1959) to describe "the region above the ionosphere in which the magnetic field has dominant control over the motions of gas and fast charged particles." ► Figure 6-1 presents a schematic of the Earth's magnetosphere showing the major regions.

Planetary magnetospheres are embedded in the solar wind, which is the outward expansion of the solar corona. At the Earth's orbit, the solar wind has an average speed of about 400 km/s. The density of particles (mainly electrons and protons with a few percent alpha particles) is observed to decrease (from values of about $3\text{--}10\text{ cm}^{-3}$ at Earth) as the inverse square of the distance from the Sun, consistent with a steady radial expansion of solar gas into a spherical volume. The solar wind speed, while varying between 300 and 700 km/s, always greatly exceeds the speed of waves characteristic of a low density, ionized, and magnetized gas (Alfvén waves). The planetary bow shock formed upstream of an obstacle in the super-Alfvénic solar wind flow can be described in fluid terms as a discontinuity in bulk parameters of the solar wind plasma in which mass, momentum, and energy are conserved. Entropy, however, increases as the flow traverses the shock with the solar wind being decelerated and heated so that the flow can be deflected around the magnetosphere. Thus, a shock requires dissipative processes, and the presence of a magnetic field allows dissipation to occur on a scale much smaller than the scale length for collisions between solar wind particles. Although planetary bow shocks do not play a significant role in processes occurring inside the magnetosphere, the crossings of spacecraft through planetary bow shocks have provided an opportunity to study the exotic plasma physics of high Mach number collisionless shocks that cannot be produced in the laboratory (see reviews by Lembege et al. 2004; Balogh et al. 2005; Treumann 2009).

Well before (Biermann 1957) provided cometary evidence of a persistent solar wind, Chapman and Ferraro (1930) considered how a strongly magnetized body would deflect a flow of particles from the Sun. They estimated the location of the stagnation point where the dynamic pressure of the solar wind ($\rho_{sw} V_{sw}^2$) is balanced by the internal pressure of the planet's magnetic field (treating the boundary as impenetrable and ignoring any contributions to internal pressure from particles). • Equation 6.4 shows that the dipole field strength as a function of radial distance (in the equatorial plane) is

$$B(r) = B_o (R_p/r)^3 \quad (6.5)$$

so that the planetary magnetic pressure varies as

$$B^2/2\mu_o = (B_o^2/2\mu_o)(R_p/r)^6. \quad (6.6)$$

For the case of a dipolar magnetic field (with poles perpendicular to the solar wind direction), the Chapman-Ferraro stagnation distance R_{CF} is

$$R_{CF} = \xi (B_o^2/2\mu_o \rho_{sw} V_{sw}^2)^{1/6}, \quad (6.7)$$

where ξ is a numerical factor that corrects for the effects of electrical currents that flow along the magnetopause (discussed in textbooks such as Cravens 1997; Kivelson and Russell 1995). Some prefer to define R_{CF} with $\xi = (2)^{1/3}$ (e.g., Vasyliunas 2009). Empirically, ξ is found to be about a factor of 1.4 to be consistent with the actual distance of the subsolar magnetopause distance (R_{MP}) at Earth (Walker and Russell 1995).

• Table 6-1 shows that R_{CF} is a reasonable approximation to the observed magnetospheric scale R_{MP} except in the case of Jupiter (and a lesser extent Saturn), where substantial plasma pressure inside the magnetosphere expands the magnetopause to roughly twice the standoff distance of a dipole (discussed in • Sect. 2.4.1). • Figure 6-4 illustrates the huge range in scale of the planetary magnetospheres. The magnetospheres of the giant planets encompass most of their extensive moon systems, including the four Galilean moons of Jupiter as well as Titan (Saturn) and Triton (Neptune). Earth's Moon, however, resides almost entirely outside

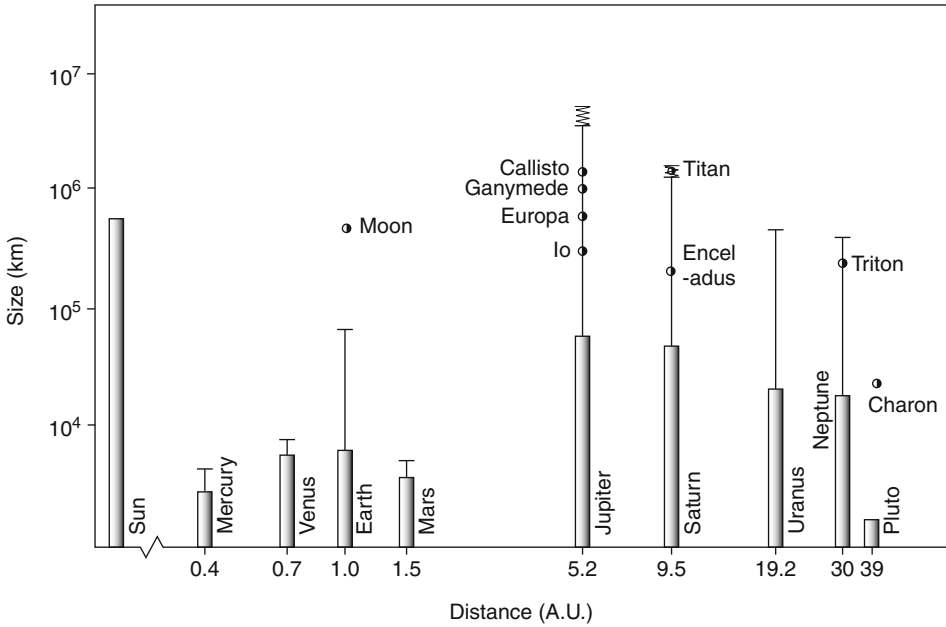
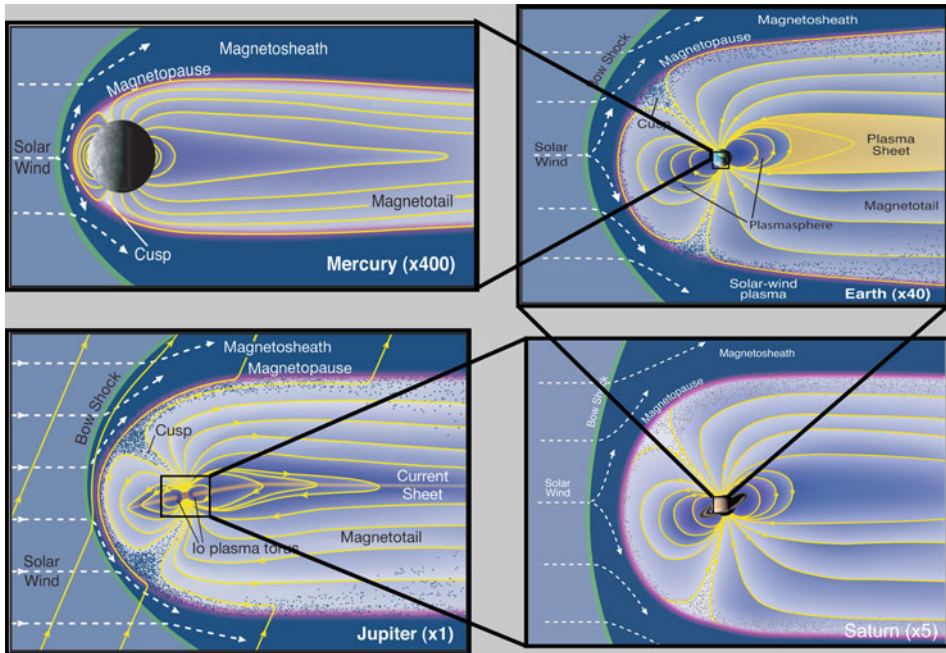


Fig. 6-4 A logarithmic plot of size of object vs. distance from the Sun for the planets (solid bars), their magnetospheres (RMP, thin bars) and the orbital radii of their primary moons. The range in sizes of the magnetospheres of Jupiter and Saturn are shown by zig-zag lines

the magnetosphere, spending less than 5% of its orbit crossing the magnetotail. **Figure 6-5** illustrates the vast range in scales: Each magnetosphere fits into the volume of the next-larger planet. Earth tends to be considered as the standard of comparison for other magnetospheres. It is natural that our home planet’s magnetosphere is better explored and its vicissitudes studied in detail, but it is also important to test our understanding of the magnetospheric principles derived at Earth by applying these concepts to other planets.

Finally, when we discuss the dynamics of magnetospheres, it will be clear that an important factor is the orientation of the planet’s magnetic field relative to the interplanetary magnetic field (**Table 6-2**). The obliquity is the angle of the planet’s spin axis relative to the ecliptic plane normal. As a planet orbits the Sun, if it has a large obliquity, it will experience not only large seasonal changes but also a wide range in angles between the upstream solar wind (and embedded IMF) and the planet’s magnetic field. Moreover, the large tilt of Uranus’ and Neptune’s magnetic fields with respect to their spin axes means that these magnetospheres also see a modulation of this solar wind angle over their spin period (i.e., a planetary day). While the solar wind remains flowing within a few degrees of radial from the Sun, the IMF forms a spiral of increasingly tangential field. At Earth the average spiral angle is 45°, at Jupiter it averages 80°, and at farther planets the field is basically tangential to the planet’s orbit. The polarity changes several times during the ~25-day solar rotation (more frequently during solar maximum). Important for the influence of the solar wind on magnetospheric dynamics are the variations in the north–south component of the IMF (which fluctuates about the ecliptic plane) and changes in solar wind ram pressure



■ Fig. 6-5
Scaling of the magnetospheres from Mercury, Earth, Saturn, to Jupiter

impacting the magnetosphere. Other factors such as the Alfvén Mach number of the incoming solar wind and plasma pressure on either side of the magnetopause also play roles that are being explored in current research (La Belle-Hamer et al. 1995; Swisdak et al. 2003; Cassak and Shay 2011).

2.3 Plasma Sources

The plasma found in a planetary magnetosphere could have a variety of sources: it could have leaked across the magnetopause from the solar wind, it may have escaped the planet's gravity and flowed out of the ionosphere, or it may be the result of the ionization of neutral material coming from satellites or rings embedded in the magnetosphere. The study of the origin of plasma populations and their evolution as they move through the magnetosphere is a detective story that becomes more complex the deeper one delves (e.g., review of Earth's plasma sources by Moore and Horwitz 2007).

The clearest indicator of which source is responsible for a particular planet's magnetospheric plasma is chemical composition (☉ Table 6-3). For example, the O^+ ions in the Earth's magnetosphere must surely have come from the ionosphere, and the sulfur and oxygen ions at Jupiter have an obvious origin in Io's volcanic gases. But the source of protons is not so clear – protons could be either ionospheric (particularly for the hydrogen-dominated gas giants), dissociation of water ejected from icy satellites, or from the solar wind. One might consider that a useful source diagnostic would be the abundance of helium ions. Emanating from the hot (millions

Table 6-3
Plasma characteristics of planetary magnetospheres

	Ganymede	Mercury	Earth	Jupiter	Saturn	Uranus	Neptune
Max. plasma density (cm^{-3})	~400	~1	4,000	~3,000	~100	3	2
Neutral density (cm^{-3})	–	–	–	~50	~1,000	–	–
Major ion species	O^+, H^+	H^+	O^+, H^+	$\text{O}^{n+}, \text{S}^{n+}$	$\text{O}^+, \text{W}^+, \text{H}^+$	H^+	N^+, H
Minor ion species		O^+, Na^+		H^+, H_3^+	H^+, H_3^+		
Dominant source	Ganymede	Solar wind	Ionosphere ^d	Io	Enceladus	Atmosphere	Triton
Neutral source ^e (kg/s)			600–2,600	70–750			
Plasma source ^f (kg/s)	5	~5	5	260–1,400	12–250	0.02	0.2
Plasma source (ions/s)	10^{26}	10^{26}	2×10^{26}	$>10^{28}$	$3\text{--}5 \times 10^{26}$	10^{25}	10^{25}
Lifetime	Minutes	Minutes	hours-days ^g	20–80 days	30–50 days	1–30 days	~1 day

^aWater-group ions from ionization, dissociation, and recombination of water ($\text{OH}^+, \text{H}_2\text{O}^+, \text{H}_3\text{O}^+$)

^bMercury's tenuous atmosphere is a likely source of heavy ions

^cThere probably are ionospheric and solar wind sources but how they compare to satellite sources is not known

^dIonospheric plasma dominates the inner magnetosphere with solar wind sources being significant in the outer regions

^eNet loss of neutrals from satellite/ring sources (Bagenal and Delamere 2011)

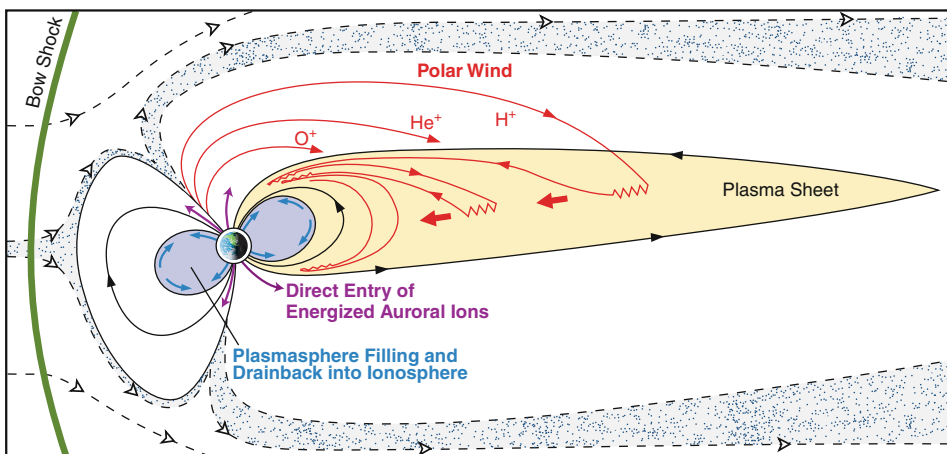
^fNet production of plasma production (Bagenal 1992; Bagenal and Delamere 2011)

^gTypical residence time in the magnetosphere. Plasma stays inside the plasmasphere for days but is convected through the outer magnetosphere in hours

of kelvins, a few hundred eV) solar corona, helium in the solar wind is fully ionized as He^{++} ions and comprises $\sim 3\text{--}5\%$ of the number density. Ionospheric plasma is much cooler (thousands of kelvins, <0.1 eV), so that ionospheric helium ions are mostly singly ionized. Thus, a measurement of the abundance ratios $\text{He}^{++}/\text{H}^+$ and He^+/H^+ would clearly distinguish the relative importance of these sources. Unfortunately, measuring the composition to such a level of detail is difficult for the bulk of the plasma, with energies in the range $1\text{ eV--}1\text{ keV}$ (e.g., Young 1997a, b, 1998). Measurement of composition is more feasible at higher energies, but then one needs to consider whether the process that has accelerated the ions within the magnetosphere, since they left the source region, is mass or charge dependent.

The temperature of a plasma can also be an indicator of its origin. Plasma in the ionosphere has characteristic temperatures of <0.1 eV; the ionization of neutral gases produces ions with energies associated with the local plasma flow speed, while material that has leaked in from the solar wind tends to have energies of a few keV. But, again, we need to consider carefully how a parcel of plasma may have heated or cooled as it moved through the magnetosphere to the location at which it is measured. **► Figure 6-6** illustrates various ways in which ionospheric plasma enters the Earth's magnetosphere and evolves by different processes. As we explore other magnetospheres, we should expect similar levels of complexity.

► Table 6-3 summarizes the main plasma characteristics of the six planetary magnetospheres. To a first approximation, one can say that escape of material from the satellites dominates the magnetospheres of Jupiter, Saturn, and Neptune, with ionospheric sources being secondary. Uranus having fewer, smaller, satellites; its weak ionospheric source probably supplies the main contribution. With only the most tenuous of exospheres, Mercury's magnetosphere contains mostly solar wind material, but energetic particle and photon bombardment of the surface may be a significant source of O^+ , Na^+ , K^+ , Mg^+ , etc. (Slavin 2004). At Earth, the net sources from the solar wind and ionosphere are probably comparable, though the most recent studies suggest that the ionospheric contribution seems to be dominant (e.g., Moore and Horwitz 2007).



■ Fig. 6-6

Sources of plasma the Earth's magnetosphere (after Chappell 1988). The *shaded, dotted area* illustrates the boundary layer through which the solar wind plasma enters the magnetosphere

2.4 Plasma Dynamics

First we describe how charged particles move in response to specified electric \mathbf{E} and magnetic \mathbf{B} fields. Depending on the situation, a range of approaches can be taken, from treating each particle separately to regarding the plasma as a magnetized fluid, plus hybrid approaches in between. The particle approach is usually appropriate for very energetic particles (e.g., trapped in radiation belts). To model plasma behavior over larger spatial and temporal scales (e.g., global magnetospheric models), it is generally appropriate to use magnetohydrodynamics (MHD). Then there are some situations where electrons can be treated as a fluid but ions need to be treated as particles (e.g., in modeling the interaction with some of the satellites). The basic physics of space plasmas is described in textbooks such as Kivelson and Russell (1995), Gurnett and Bhattacharjee (2005), Gombosi (1998), or Cravens (1997).

After describing the motions of energetic particles in dipole magnetic fields close to the planet, the radiation belts of the major magnetospheres are compared and their properties listed in [Table 6-4](#). Moving farther away from the planet, the magnetic field becomes weaker and can be modified from a simple dipole by electrical currents flowing through the plasma. Theoretical ideas are applied to the different planetary magnetospheres to determine where and when plasma flows are predominantly rotation with the planet vs. controlled by the interaction of the solar wind with the magnetosphere. [Table 6-5](#) lists various dynamical parameters of the different planetary magnetospheres that quantify the relative importance of rotational vs. solar wind influences in each case.

When comparing the dynamics of different magnetospheres, the traditional approach has been to compare electric fields and electric currents (i.e., \mathbf{E} , \mathbf{J}). Over the past decade, the case has been made (Parker 2007; Vasyliūnas 2001, 2011) that such an “electrical circuit” approach is only valid for quasi-static situations (specifically, where temporal changes occur over time scales that are long compared with the transit time of Alfvén waves across the system) and that one should derive the flows and magnetic fields (\mathbf{B} , \mathbf{v}) resulting from the various stresses on the system. This review presents the traditional (\mathbf{E} , \mathbf{J}) approach partly because it is the one that dominates the current literature but also because it is perhaps easier to explain the interactions between different components of a complex system.

■ **Table 6-4**

Energetic particle characteristics in planetary magnetospheres

	Earth	Jupiter	Saturn	Uranus	Neptune
Phase space density ^a	20,000	200,000	60,000	800	800
Ring current ^b ΔB (nT)	10–23	200	10	<1	<0.1
Plasma β ^c	<1	10–100	1–5	~0.1	~0.2
Auroral power (W)	10^{10}	10^{12}	10^{11}	5×10^9	2–8 $\times 10^7$

^aThe phase space density of energetic particles (in this case 100 MeV/G ions) is measured in units of $c^2(\text{cm}^2 \text{ s sr MeV}^3)^{-1}$ and is listed near its maximum value (Cheng et al. 1987; Mauk et al. 1995)

^bThe magnetic field produced at the surface of the planet due to the ring current of energetic particles in the planet’s magnetosphere

^cThe ratio of the thermal pressure to magnetic pressure of a plasma, $\beta = nkT/(B^2/2\mu_0)$. These values are typical for the body of the magnetosphere. Higher values are often found in the tail plasma sheet and, in the case of the Earth, at times of enhanced ring current

■ Table 6-5

Dynamical characteristics of planetary magnetospheres

	Mercury	Earth	Jupiter	Saturn	Uranus	Neptune
R_{MP}^a (km)	4,000	6.5×10^4	6×10^6	1×10^6	6×10^5	6×10^5
V_{sw}^b (km/s)	370	390	420	430	450	460
t_{N-T}^c	10 s	3 min	4 h	45 min	20 min	20 min
R_T^d (R_p)	3	20	170	40	50	50
R_T^d (km)	8,000	1.3×10^5	1.2×10^7	2.3×10^6	1.3×10^6	1.2×10^6
$V_{rec,1}^e$ (km/s)	40	22	16	16	16	16
$V_{rec,2}^f$ (km/s)	37	39	42	43	45	46
t_{rec}^g	3 min	1 h	80 h	15 h	8 h	7 h
d_x^h (R_p)	30	200	1,700	400	500	500
$V_{co}/V_{rec,2}^i$	4×10^{-5}	0.04	8	1.3	0.4	0.4
R_{pp}^j (R_p)	0.03	6.7	350	95	70	70

^aSubsolar magnetopause distance

^b $V_{sw} = 387(a_p/a_E)^{0.05}$ (km/s) from Belcher et al. (1993)

^cSolar wind nose-terminator time: $t_{N-T} = R_{MP} / V_{sw}$

^dRadius of cross section of magnetotail, approximated as $R_T = 2R_{MP}$

^eReconnection speed assuming 20% reconnection efficiency and $v_{rec} \sim 0.2 v_{sw} B_{sw} / B_{MP}$ km/s (e.g., Kivelson 2007)

^fReconnection speed assuming 10% reconnection efficiency and $v_{rec} \sim 0.1 v_{sw}$ km/s

^gReconnection time $t_{rec} = R_T / v_{rec,2}$ (s)

^hDistance to X-line $d_x \sim v_{sw} t_{rec}$

ⁱAssumes rotation speed at the magnetopause is ~30% of rigid corotation

^jDistance to plasmopause, where corotation is comparable to reconnection flow (e.g., Kivelson 2007)

2.4.1 Energetic Particles and Radiation Belts

A particle with charge q , mass m , and velocity v in an electric field E and magnetic field B experiences a Lorentz force which causes the particle to accelerate

$$F = q(E + v \times B) = mdv/dt, \quad (6.8)$$

Solving (6.8) is relatively straightforward if E and B are specified. For the case of a dipole magnetic field, charged particles exhibit motions on three temporal and spatial scales, as illustrated in Fig. 6-7a. On the shortest time scale, particles gyrate about the magnetic field with a gyroradius of

$$R_g = mv_{\perp}/qB, \quad (6.9)$$

where v_{\perp} is the speed of the particle perpendicular to the magnetic field. Positively and negatively charged particles gyrate in opposite directions. As a particle moves along the magnetic field, it experiences stronger magnetic field as it approaches the poles. In stronger fields, the gyromotion is increased and, through conservation of total energy, the particle motion along the field decreases. Thus, the particle is trapped and “bounces” between polar regions of stronger fields. On longer time scales, the particles experience drifts around the planet (Fig. 6-7a) producing a “belt” of trapped particles.

The particle source and loss processes act on much longer time scales (hours–years at Earth, months–years at Jupiter). Radial (cross-field) motions are diffusive – mostly scattering by small-scale perturbations in the magnetic field. Ultimately, the particles eventually escape

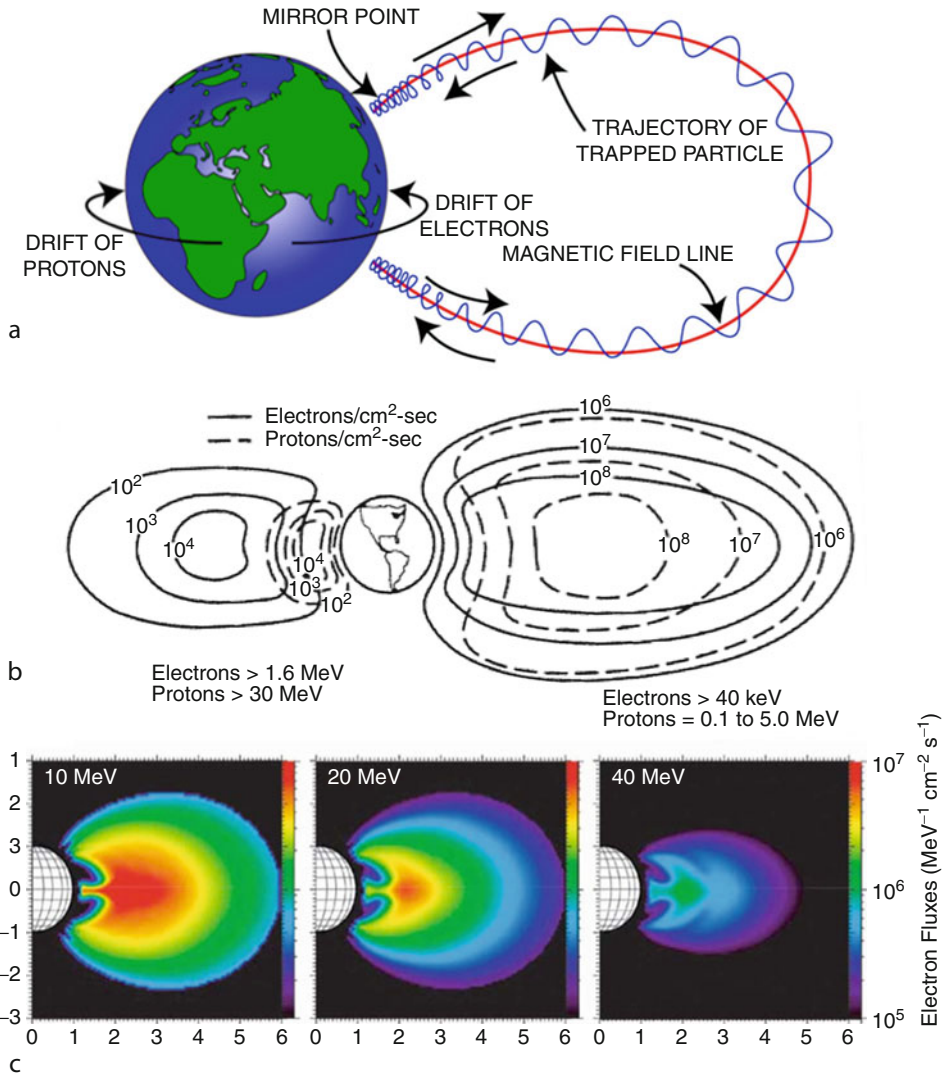


Fig. 6-7
 (a) Radiation belt dynamics. Flux of radiation belt particles at (b) Earth (from Walt 2005) and (c) Jupiter (From Santos-Costa and Bourdarie 2001)

the magnetosphere, charge exchange with neutral particles (producing energetic fast neutrals that escape the system), or are lost by hitting moons or the planet’s atmosphere.

Figure 6-7b shows typical fluxes of energetic electrons and protons measured in the Earth’s radiation belts (for introductory text see Walt 2005). The higher energy particles (few-100s MeV, left of Fig. 6-7b) are produced via a process called cosmic ray albedo neutron decay (CRAND, whereby neutrons generated by cosmic rays bombarding the atmosphere decay to produce protons and electrons) and are confined closer to the planet. The lower energy particles (10s–100s KeV, right of Fig. 6-7b) are “injected” into the inner magnetosphere from the

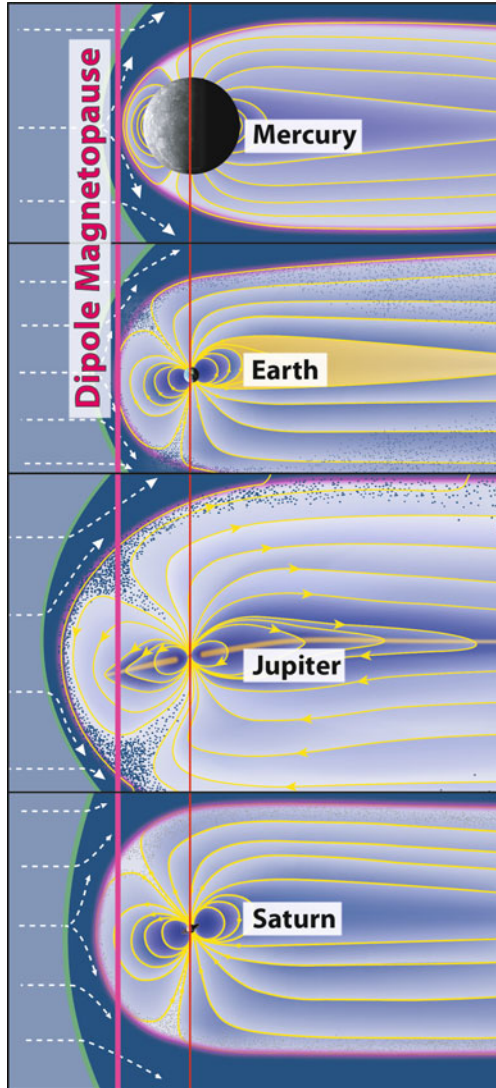
magnetotail during magnetic storms, dominate the particle energy density, and carry the ring current. Luckily, the most useful orbits for satellites (low Earth orbit and geosynchronous orbit at $6.6 R_{\text{Earth}}$) generally avoid the radiation belts, but at times of high geomagnetic activity, sensitive electronics as well as astronauts can be exposed to significant fluxes of damaging energetic particles.

As the discovery of Earth's radiation belts marked the dawn of the space age, the nearly simultaneous detection of radio emission from Jupiter in the late 1950s started the exploration of the jovian magnetosphere. The radiation belts of Jupiter have been observed via radio emission from MeV electrons which generate intense synchrotron emission at decimetric wavelengths observed from Earth-based radio telescopes as well as by the Cassini spacecraft on its way to Saturn (see the review by Bolton et al. 2004).  *Figure 6-7c* shows the distribution of energetic electron fluxes at 10, 20, and 40 MeV derived from modeling emissions at different wavelengths (Santos-Costa 2001). These high fluxes of energetic electrons (and the accompanying energetic ions) provide a quick, lethal dose to sensitive electronics so that spacecraft aimed close to Jupiter need to avoid and/or be protected against high radiation doses. Such a mission, Juno, will go into polar orbit in the summer of 2016, skimming over Jupiter's clouds and ducking under the radiation belts.

The smaller physical scale and shorter time scales of the Saturn system result in less net acceleration and weaker fluxes of energetic particles. Absorption by the majestic ring system further prevents the buildup of comparable fluxes close to the planet, so that there are no belts emitting synchrotron radiation at Saturn. Significant populations of energetic particles were detected at Uranus and Neptune, but the fluxes were much lower than at Jupiter and Saturn. It could be that the shorter residence times in these smaller magnetospheres limit the amount of acceleration, or it may be much harder for particles to be stably trapped in such non-dipolar fields. The trapped populations of energetic particles in the magnetospheres of the major planets are compared by Cheng et al. (1987), Mauk et al. (1995), and Mauk and Fox (2010). In the mini-magnetospheres of Ganymede and Mercury, the time scales for energetic particles to drift around these objects are only minutes, suggesting that particles are not stably trapped (see review by Kivelson 2007).

In the cases of all the giant planets, the observed high fluxes of energetic particles in the middle magnetosphere and compositional evidence imply that some fraction of the thermal plasma is accelerated to high energies, either by tapping the rotational energy of the planet (in the cases of Jupiter and Saturn) or by processes in the non-dipolar fields of the tail (at Earth and probably Uranus and Neptune). If the energy density of the energetic particle populations is comparable to the magnetic field (i.e., $\beta > 1$ where $\beta = nkT/(B^2/\mu_0)$, as shown in  *Table 6-4* for Jupiter and Saturn), then particle pressures inflate and stretch out the magnetic field and generate strong currents in the equatorial plasma disk. While Uranus and Neptune have significant radiation belts, the energy density remains small compared with the magnetic field (i.e., $\beta \ll 1$, see  *Table 6-4*).

 *Figure 6-8* compares the magnetospheres of Mercury, Earth, Saturn, and Jupiter which are scaled to the Chapman-Ferraro distance ( *Sect. 2.2*) that assumes the internal plasma pressure is negligible and that the planetary field is a dipole.  *Figure 6-8* illustrates how the substantial plasma pressure inside at Jupiter (and to a lesser extent at Saturn) expands the magnetosphere. At Jupiter, the high plasma pressures in the plasma sheet dominate the local magnetic field pressure, producing values of β greater than unity beyond $\sim 15 R_J$, increasing to greater than 100 at $45 R_J$ (Mauk et al. 2004). Not only does the plasma pressure dominate the magnetic pressure, but the radial profile of plasma pressure is also considerably flatter than the $R^{-1/6}$ variation in



■ Fig. 6-8

Magnetospheres of Mercury, Earth, Jupiter, and Saturn scaled to the distance of the magnetopause for a dipole field (based on Chapman and Ferraro 1930). Jupiter and Saturn have extended magnetospheres due to the significant plasma pressure inside

magnetic pressure for a dipole field. It is the high plasma pressure in the plasma disk that doubles the scale of Jupiter's magnetosphere from the dipolar stand-off distance of $\sim 42 R_J$ to $65\text{--}90 R_J$. A simple pressure balance between the ram pressure of the solar wind and the magnetic pressure of a dipole produces a weak variation in the terrestrial dayside magnetopause distance R_{MP} for a solar wind density ρ and speed v_{sw} such that $R_{MP} \propto (\rho v_{sw}^2)^{-1/6}$. Measurements of the magnetopause locations at Jupiter indicate a much stronger variation, $R_{MP} \propto (\rho v_{sw}^2)^{-1/4.5}$

(Slavin et al. 1985; Huddleston et al. 1998; Joy et al. 2002; Alexeev and Belenkaya 2005). Consequently, a factor 10 variation in ram pressure at Earth changes the magnetopause distance by only 70%, while at Jupiter, the tenfold variations in solar wind pressure often observed at 5 AU cause the dayside magnetopause to move between $\sim 100R_J$ and $\sim 50R_J$. At Saturn, the plasma pressures are less than Jupiter but the plasma beta is still greater than unity beyond 8 Rs (e.g., Sergis et al. 2010) and has values of 2–5 in the plasma sheet. The more modest values of beta at Saturn are consistent with the magnetopause standoff distance varying as $-1/5$ power of solar wind pressure, as found by Kanani et al. (2010).

2.4.2 Rotational Flows

Magnetospheric configuration is generally well described by MHD in which the magnetic field can be considered frozen into the plasma flow. Thus, we need to consider the processes controlling magnetospheric flows. The two largest sources of momentum in planetary magnetospheres are the planet's rotation and the solar wind. The nature of large-scale circulation of material in the magnetosphere depends on which momentum source is tapped. For planetary magnetospheres, corotation of plasma with the planet is a useful first approximation with any departures from strict corotation occurring when certain conditions (described below) break down. It may be helpful to think of plasma in the magnetosphere as mass that is coupled by means of magnetic field lines to a giant flywheel (the planet) with the ionosphere (or magnetosphere just above) acting as the clutch.  *Figure 6-9* illustrates the dynamical process whereby the magnetospheric plasma is coupled to the angular momentum of the spinning planet (for a detailed mathematical description and further references see Vasylunas 1983). The region within a magnetosphere where the flow is predominately rotational is called the *plasmisphere*.

For a magnetospheric plasma to rotate with the planet, the upper region of the neutral atmosphere must corotate with the planet and be closely couple to the ionosphere by collisions. The electrical conductivity of the ionosphere σ^i is large so that in a corotating ionosphere (with velocity V^i), any horizontal currents (perpendicular to the local magnetic field) are given by Ohm's law

$$J_{\perp}^i = \sigma^i (E^i + V^i \times B). \quad (6.10)$$

Just above the ionosphere where the conductivity perpendicular to the magnetic field in the (collision-free) magnetosphere, σ_{\perp}^m is essentially zero and $E^m = -V^m \times B$. Because the plasma particles are far more mobile in the direction of the local magnetic field, the parallel conductivity σ_{\parallel}^m is large and the field lines can be considered to be equipotentials ($\mathbf{E} \cdot \mathbf{B} = 0$). Thus, the electric field in the magnetosphere can be mapped into the ionosphere ( *Fig. 6-8a*). Because the ionosphere is relatively thin, the electric field E^m just above the ionosphere is the same as E^i so that we can write

$$J_{\perp}^i = \sigma^i (V^i - V^m) \times B, \quad (6.11)$$

The condition for the corotation of the magnetospheric plasma is that the ratio J_{\perp}^i / σ^i be sufficiently small so that

$$V^m = V^i = \Omega \times R. \quad (6.12)$$

The corotational electric field is therefore

$$E_{\text{cor}} = -(\Omega \times R) \times B_{\text{planet}}. \quad (6.13)$$

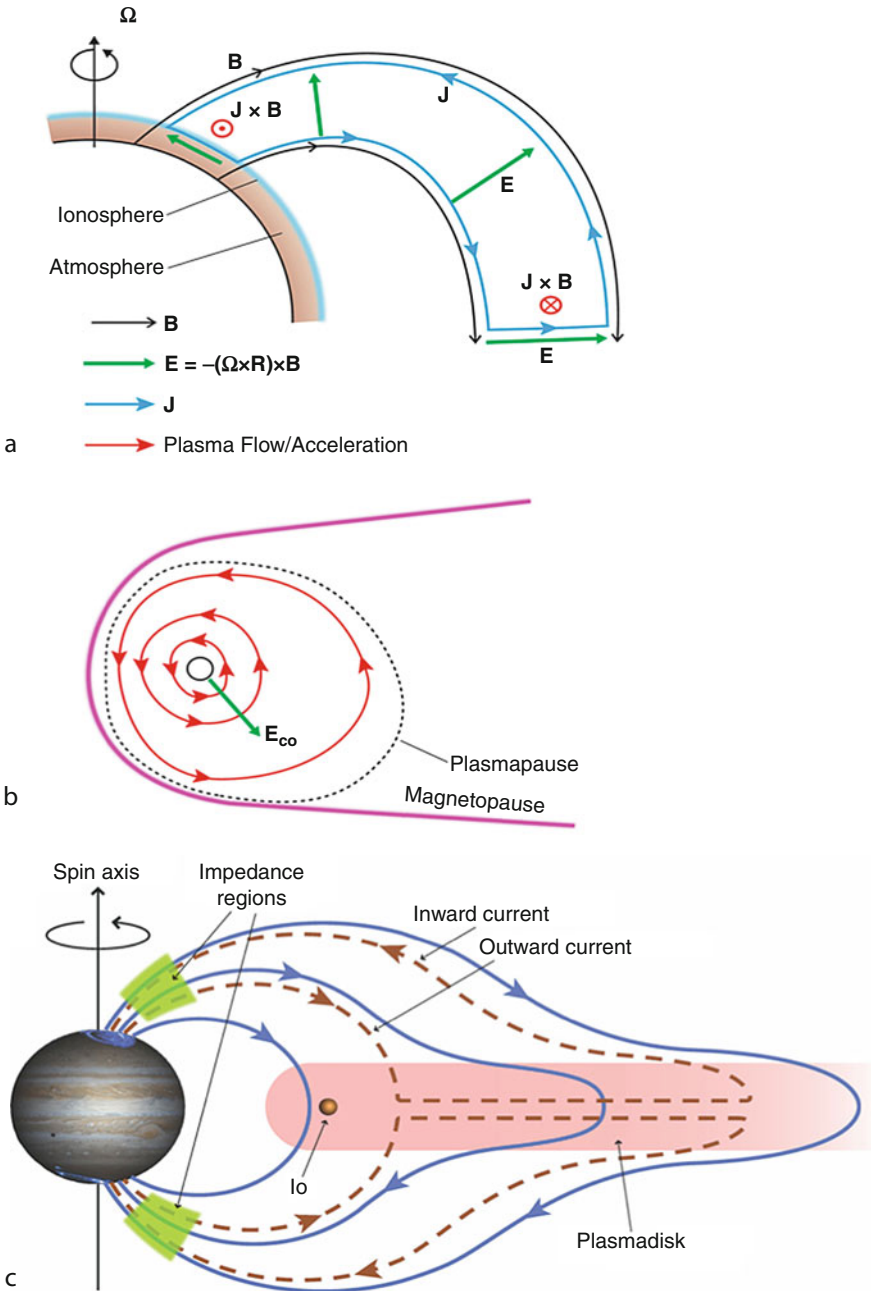


Fig. 6-9

Dynamics of rotation-dominated magnetospheres. (a) The electrodynamics in the meridional plane. (b) Dynamics in the equatorial plane. The plasmopause separates rotation-driven flows (in the plasmasphere) from solar-wind-driven flows outside. (c) In a magnetosphere where rotation confines the plasma to the equator (as illustrated at Jupiter) there is a lack of charged particles able to carry electrical currents along the magnetic field. Based on experience at Earth, it is expected that this leads to the development of regions of high impedance at high latitudes

For a dipolar magnetic field that is aligned with the rotation axis, the corotational electric field (in the equatorial plane, see [Fig. 6-9b](#)) is radial with magnitude

$$E_{\text{cor}} = \Omega B_0 / r^2. \quad (6.14)$$

It is clear that large ionospheric conductivities facilitate corotation. A large σ_{\parallel}^m also means that any currents in the magnetosphere that result from mechanical stresses on the plasma are directly coupled by field-aligned currents to the ionosphere. Thus, corotation breaks down when mechanical stresses on the magnetospheric plasma drive ionospheric currents that are sufficiently large for the ratio J_{\perp}^i / σ^i to become significant. Such conditions might occur in regions where there are large increases in mass density due to local ionization of neutral material, where there are strong radial motions of the plasma, or where external stresses begin to influence the magnetospheric plasma. When the magnetosphere imposes too large a load, the ionospheric clutch begins to slip.

The above argument, originally made by Brice and Ioannidis (1970), quantified by Hill (1979), and reviewed by Vasyliunas (1983) and Mauk et al. (2009), assumes that there are plenty of particles around to carry any currents between the magnetosphere and the ionosphere. In magnetospheres that are dominated by rotation, centrifugal forces confine the ions (which pull in the electrons electrostatically) to the region along a magnetic flux tube that is farthest from the rotation axis. The net results are to stretch the magnetic field in the equator (see [Fig. 6-9c](#)) and to limit the electrical conductivity along the field line (σ_{\parallel}^m). Consequently, significant parallel electric fields develop in the magnetosphere, probably confined to small regions quite close to the planet, labeled impedance regions in [Fig. 6-8c](#) (Mauk et al. 2002; Ergun et al. 2009; Ray et al. 2009, 2010). Such parallel electric fields accelerate electrons into the atmosphere (in regions of upward current) where they trigger strong auroral emissions. Thus, the region where corotation with the planet begins to break down can be associated with bright aurora (see review by Clarke et al. 2005).

Because the plasma is magnetically trapped in a rotation-dominated magnetosphere, transport away from the source implies either inward or outward radial transport across the magnetic field. In a magnetosphere that is dominated by rotation, outward transport is energetically favored over inward transport. As plasma builds up (e.g., from ionization of material coming from moons), it becomes energetically favorable for magnetic flux tubes laden with plasma to interchange with outward neighbors that contain less plasma. This process of flux tube interchange is thought to be responsible for transport of plasma on times scales of weeks through the giant magnetospheres, but the exact process and the mechanisms that control the radial transport rate are far from understood in detail (see review in Thomas et al. 2004). Furthermore, one expects plasma that expands into a larger volume to become colder as it moves outward. Yet the plasmas at both Jupiter and Saturn are hotter at larger radial distance. The issue of what is heating the plasmas of these magnetospheres remains a major conundrum of planetary magnetospheres (see review by Bagenal and Delamere 2011).

2.4.3 Global Solar-Wind-Driven Convection

Next, let us consider how the momentum of the solar wind is harnessed by processes occurring near the magnetopause. In the early 1960s, there was a debate about how these processes operate. Axford and Hines (1961) proposed a viscous interaction at the magnetopause boundary.

This idea was dismissed for the Earth because (a) people could not see how collisionless plasmas could have “viscosity” and (b) the observations supported the alternative idea. Recently, there has been a revival of interest in small-scale processes that might act like an effective viscosity, and we shall return to such ideas at the end of this section. In the meantime, Dungey (1961) showed how, under certain conditions, the solar magnetic field interconnects with the planetary magnetic field.  [Figure 6-10](#) shows how reconnection of the planet’s magnetic field with the interplanetary field harnesses the momentum of the solar wind and drives the circulation of plasma within the magnetosphere; this circulation is sometimes called the Dungey cycle.

The first task is to quantify the spatial and temporal scales over which the Dungey cycle operates at each planet. The actual process of reconnection (where adjacent magnetic field lines of different orientations are “cut and reconnected” as in steps 1 and 6 of  [Fig. 6-9](#)) is a plasma process that occurs on very small scales. Reconnection proceeds when the IMF brought to the magnetopause by the solar wind has a component of the embedded magnetic field that is antiparallel to the planetary magnetic field just inside the magnetopause (step 1). The reconnected flux tubes is limited to relatively small structures – flux transfer events (FTEs) – whose recurrence and fractional scale on the magnetopause decreases as the Alfvén Mach number of the flow seems to increase, consistent with a lower rate of magnetic flux being convected into the magnetopause (see Jia et al. (2010b) for a comparison of FTEs at different planets). Magnetic reconnection efficiency can be strongly reduced in high (>10) magnetosonic Mach solar wind flows due to the dominance of plasma pressure forces over magnetic forces (Scurry and Russell 1991; Scurry et al. 1994), though (Grocott et al. 2009) found, no evidence for a significant reduction. The factors controlling the reconnection efficiency of the IMF and planetary fields are active areas of research (La Belle-Hamer et al. 1995; Swisdak et al. 2003; Cassak and Shay 2011).

 [Figure 6-10](#) shows that the reconnected field lines (e.g., 2 and 7) are “bent” indicating strong currents and tension forces. While the microscale process that initiates the reconnection is dissipative, the net result is the release of considerable magnetic tension that accelerates plasma from the reconnection point, generating beams of energetic particles. Reconnection is a major source of energy in the solar corona as well as a source of energetic particles in the Earth’s magnetosphere.

Consider the situation where some fraction of the time there is a component of the IMF that is opposite to the direction of the planetary magnetic field at the magnetopause (e.g., a negative B_z for Earth and a positive B_z for Jupiter and Saturn, ignoring the complexities of Uranus and Neptune for the moment). Such a configuration allows the reconnection of planetary and interplanetary fields at the dayside magnetopause (see step 1 of  [Fig. 6-10](#)). There is now one end of the flux tube attached to the planet and the other is out in the solar wind. To estimate how long it takes the section of flux tube in the solar wind to move to the plane of the planet’s terminator (step 3), the subsolar magnetopause distance R_{MP} is divided by the local solar wind speed V_{sw} . For  [Table 6-5](#), an empirical fit to Voyager data is used that includes a modest increase in the solar wind speed with distance from the Sun, but the basic results would not be very different if a constant value for the solar wind (say ~ 400 km/s) were used. One immediately sees the effect of the vast scale of the giant magnetospheres of the outer planets: the nose-terminator time scale, τ_{N-T} , is a mere 10 s at Mercury, 3 min at Earth, and as much as 4 h at Jupiter.

The next step is to calculate how long the open flux tube would take to convect to the equator or central plane of the magnetotail (from steps 3 to 6 in  [Fig. 6-10](#)). For simplicity, the radius of

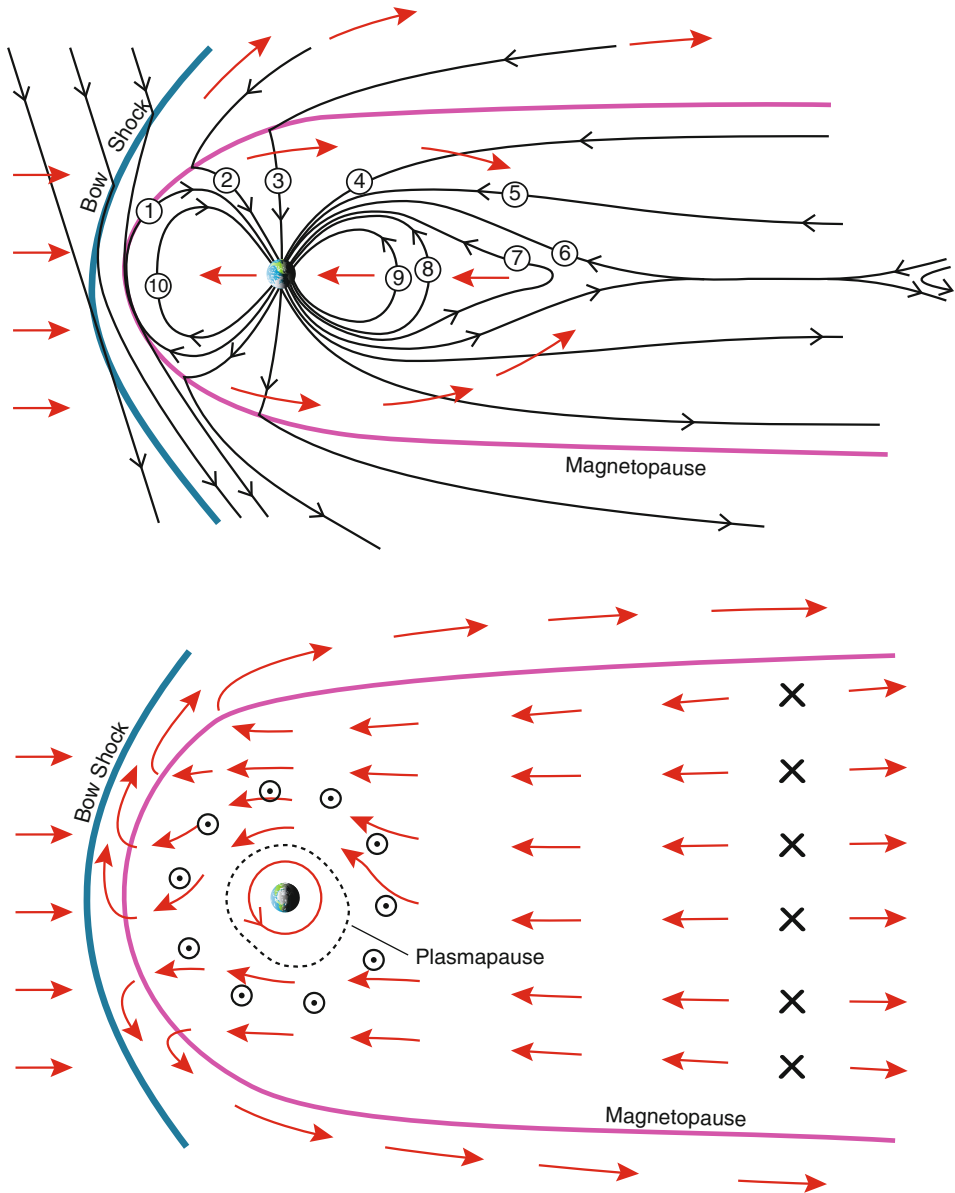


Fig. 6-10

Magnetospheric dynamics associated with the Dungey cycle driven by the solar wind. *Top*: view in the noon-midnight meridian plane. The numbers show the time sequence for a flux tube being reconnected at the dayside magnetopause and convected through the magnetosphere. *Bottom*: view in the equatorial plane (After Dungey (1961))

each magnetotail has been approximated as twice the subsolar standoff distance (i.e., $2R_{MP}$). We need to divide this distance by a convective speed to estimate a minimum convective time scale. The traditional approach to calculating the speed of circulation in the magnetosphere driven by

solar wind was to calculate the electric field associated with an object moving with the planet relative to the solar wind, $E_{sw} = -V_{sw} \times B_{IMF}$, assume that some fraction (say, 10–20%) of this electric field permeates the whole magnetosphere (i.e., the convective electric field $E_{con} \bullet 0.1-0.2 E_{sw}$), and then estimate how magnetospheric plasma would drift in this convection electric field and the local planetary magnetic field ($V_{con} = E_{con} \times B_{planet}$) (e.g., Cravens 1997).

In the meantime, to obtain a rough upper estimate for a reconnection-driven convection speed, we have taken 10% of the solar wind speed (roughly 40 km/s at all planets), corresponding to a $\sim 10\%$ reconnection efficiency. Again, the large scales of the giant planet magnetospheres mean that even with generous values for the convection speed, one obtains long time scales for flux tubes to convect to the equator from the upper and lower magnetopause boundaries. At Jupiter, this time scale is 80 h, equivalent to eight full rotation periods. The time scales for steps 3–6 of the Dungey cycle for the other giant planets are much less, but they are still several hours and comparable with the planetary rotation rate. By contrast, this convection time scale is just an hour at Earth and a few minutes at Mercury.

The Dungey cycle time scale mentioned above can also be used to estimate the length of the magnetotail, by multiplying the reconnection time scale and the solar wind speed. More accurately, it gives us the distance down the tail to the X-line, where further reconnection closes the open magnetic flux (hence conserving, on average, the total magnetic flux emanating from the planet). The re-closed magnetic flux tube then convects sunward (steps 7–10 in [Fig. 6-10](#)) to begin the Dungey cycle again at the dayside magnetopause. [Table 6-5](#) shows that values for this X-line (often called, for obscure reasons, the distant Earth neutral line). This X-line distance is about $20 R_{MP}$ if one takes the simplest formula for reconnection-driven convective speed V_{con} to be 10% of V_{sw} and the tail radius to be $2R_{MP}$. Lower estimates of V_{con} (e.g., derived including field compression by Kivelson 2007) give larger distances to the tail X-line. In practice, we know that the Earth's tail extends for several thousand R_E , while Jupiter's magnetotail was encountered by Voyager 2 as it approached Saturn at a distance greater than $9,000R_J$ or 4 AU downstream of Jupiter. The estimates of distances to magnetotail X-lines derived from simple Dungey cycle principles shown in [Table 6-4](#) illustrate the vast scales of the magnetospheres of the outer planets, and the huge distances that flux tubes reconnecting (re-closing) in the tail would need to travel back to the planet if these magnetospheres were driven by Earth-like processes.

We compared the corotation speed $V_{cor} = \Omega \times R$ with our upper estimate of the convection flows driven by reconnection, V_{con} . The very low values in [Table 6-5](#) of V_{cor}/V_{con} for Mercury and Earth confirm that the dynamics of these magnetospheres are dominated by coupling to the solar wind, while it is clearly the case that rotation dominates Jupiter and Saturn. Uranus and Neptune, once again, are not simple cases with speed ratios of order unity that would suggest the comparable importance of rotation and solar-wind-driven circulation.

In a general sense, close to the planet where the magnetic field is strong and rotation speeds are low, one expects strong coupling to the planet's rotation. At larger distances from the planet, one expects decreasing corotation and an increasing influence of the solar wind. Finally, we can estimate the size R_{pp} of a region (called the *plasmopause* at Earth) within which rotation flows dominate and outside of which the solar wind interaction drives flows. The values for R_{pp} in the bottom row of [Table 6-5](#) further illustrate how the planets' magnetospheres span the range between the extremes of Jupiter (where $R_{pp} \gg 1$ and rotation dominates throughout) and Mercury (where $R_{pp} \ll 1$ means that there is no region of corotating plasma in the tiny magnetosphere).

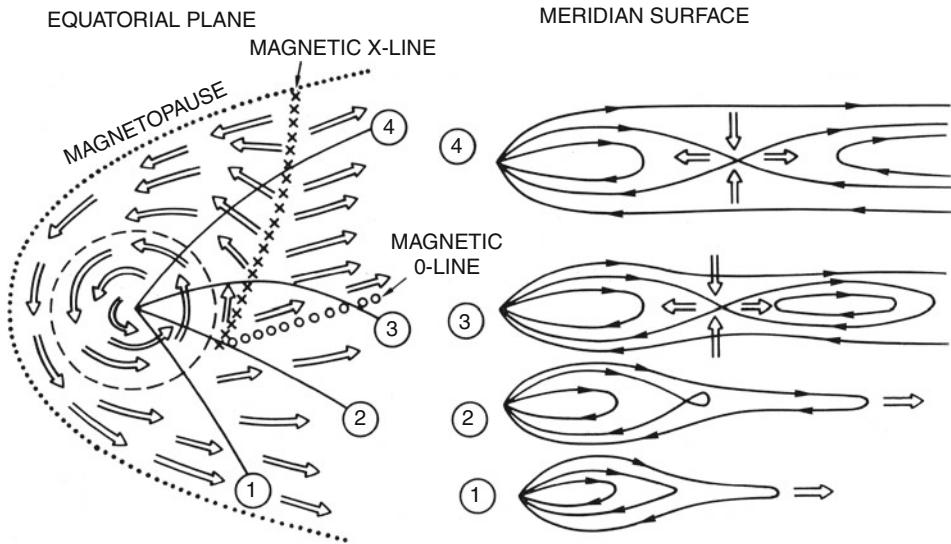
Fundamentally, dawn-dusk asymmetry of the magnetic field and plasma flows inside a planetary magnetosphere is the result of the solar wind interaction with the magnetosphere. To account for these solar-wind-driven dawn-dusk asymmetries, either a mechanism such as reconnection-driven global convection (as in the Dungey cycle above) is evoked or one might consider a mechanism more akin to the original (Axford and Hines 1961) model of a viscous interaction of the solar wind with the magnetopause boundary. Rather than a Dungey-style global cycle of reconnection (that opens planetary magnetic flux on the dayside, carries the flux tube over the poles, and closes the flux in the tail), the magnetic flux could be opened and closed intermittently in small-scale structures in turbulent interaction regions on the flanks of the magnetosphere.

So what might be responsible for viscous processes at the magnetosphere? Except in the densest locations (e.g., ionospheres), space plasmas are generally collisionless (i.e., the mean free path is larger than the typical scale of the system). Thus, it is necessary to find other dissipative processes occurring on a scale comparable to the magnetopause thickness. But there are a variety of waves, perhaps driven by shear (Kelvin–Helmholtz) instabilities or by nonequilibrium particle velocity distributions, that might act as a means for the solar wind plasma to interact with the plasma at the boundary of the magnetosphere, particularly when the magnetic field on either side of the boundary is weak. With strong contrast in flows across the magnetopause, the Kelvin–Helmholtz instability (KHI) – analogous to “wind over water” instability of hydrodynamics – is a good possibility. Observations at Earth and numerical models show that KHI vortices generate twisted magnetic fields, strong currents, and small-scale reconnections (both opening and closing flux intermittently) that allow plasma transport across the boundary (see review by Delamere and Bagenal 2010). Such a viscous process could be considered a comet-like interaction, with the IMF being temporarily “hung up” on the magnetopause, is to stretch the IMF out behind the object in an extended tail. This would mean that the magnetic field in the magnetotail would not be attached to the planet (as implied by [▶ Fig. 6-10](#) for the Dungey cycle) but has each end in the solar wind and is “kinked” where flux tubes are dragged over the magnetopause.

2.4.4 Plasmoid Ejection

The Dungey cycle of opening magnetic flux on the dayside of a magnetosphere and subsequent closing in the magnetic tail produces a pinching off of the nightside plasma sheet and ejection of magnetospheric plasma down the magnetotail (see far right of [▶ Fig. 6-10](#)). The ejection of such a blob of plasma – a *plasmoid* – involves rapid conversion of energy stored in the stretched magnetic field into kinetic energy of the ejected plasmoid as well as beams of energetic particles. Such an explosive ejection of material and the associated phenomena is called a “substorm” at Earth. Substorms occur frequently (on average several times per day) at Earth from an X-line that ranges from 8 to 20 R_E .

For a magnetosphere that is driven primarily by rotation rather than the solar wind (i.e., R_{pp} in listed in [▶ Table 6-5](#) is large), as the plasma rotates around onto the nightside, it is no longer confined by magnetopause currents, moves farther from the planet, and stretches the magnetic field with it (field line (1) in [▶ Fig. 6-11](#)). At some point, either the coupling to the planet breaks down completely (e.g., because the Alfvén travel time between the equator and the poles becomes a substantial fraction of a rotational period) or the field becomes so radially



■ Fig. 6-11

Qualitative sketch of plasma flow (*left*) in the equatorial plane and (*right*) in a sequence of meridian surfaces (locations 1, 2, 3, and 4) expected from the planetary wind model (From Vasyliunas 1983)

extended that an x-point develops and a blob of plasma detaches and escapes down the magnetotail (field lines (2), (3), and (4) in ● Fig. 6-11 from Vasyliunas 1983). Kivelson and Southwood (2005) point out that the stretched, equatorial magnetic field becomes so weak that the gyro-radii of the heavy ions becomes comparable to scales of local gradients. It is possible that the plasma diffuses across the magnetic field and “drizzles” down the magnetotail. If the process were entirely diffusive, then the magnetic flux would remain connected to the planet. The flux tubes would become unloaded and presumably shrink (“dipolarize”) as they swung around to the dayside.

It is quite possible that Dungey cycle transport of flux toward the center of the magnetotail acts in combination with rotationally driven expulsion of plasmoids (sometimes called the Vasyliunas cycle), depending on how much flux is opened by large-scale dayside reconnection and whether the opened flux tubes penetrate deep into the tail vs. being closed by reconnection on the flanks of the magnetosphere.

3 Magnetospheres of the Outer Planets

The Voyager flybys of all four giant planets allowed comparison of their magnetospheres (e.g., Bagenal 1992). While all four are dominated by rotation, they can be separated into large, regular, and fast rotators (Jupiter and Saturn) vs. irregular oblique rotators (Uranus and Neptune). We discuss each planetary magnetosphere in turn below.

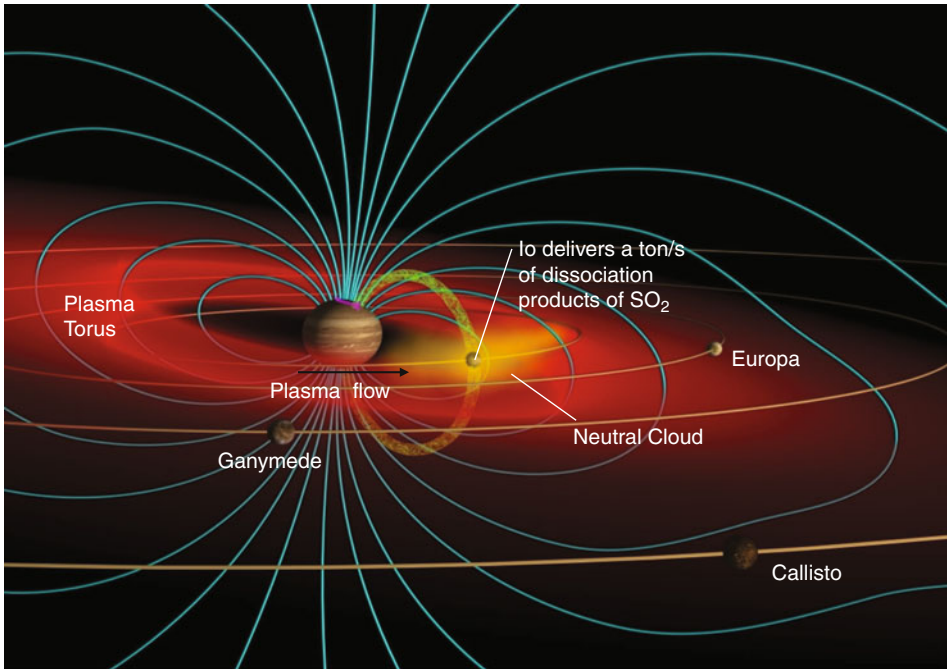
3.1 Jupiter

Jupiter is a planet of superlatives: the most massive planet in the solar system, which rotates the fastest, has the strongest magnetic field and has the most massive satellite system of any planet. These unique properties lead to volcanoes on Io and a population of energetic plasma trapped in the magnetic field that provides a physical link between the satellites, particularly Io, and the planet Jupiter. For those seeking further details, the jovian magnetosphere is reviewed in seven chapters of the book *Jupiter: The Planet, Satellites and Magnetosphere* (Bagenal et al. 2004), and only subsequent research is cited in this section.

Clear indications that Jupiter traps electrons in its magnetic field were apparent as soon as astronomers turned radio receivers to the sky. Early radio measurements showed that Jupiter has a strong magnetic field tilted about 10° from the spin axis, that energetic (MeV) electrons were trapped at the equator close to the planet, and that Io must be interacting with the surrounding plasma and triggering bursts of emission. The magnetometers and particle detectors on Pioneer 10 (1973) and Pioneer 11 (1974) revealed the vastness of Jupiter's magnetosphere and made in situ measurements of energetic ions and electrons. The Voyager 1 flyby in 1979 revealed Io's prodigious volcanic activity, thus explaining why this innermost Galilean moon plays such a strong role. Additional data came from subsequent traversals by the Ulysses (1992), Cassini (2000), and New Horizons (2007) spacecraft, but it was the 34 orbits of Galileo (1995–2003) around Jupiter that mapped out magnetospheric structures and monitored their temporal variability. As at Earth, magnetospheric activity is projected onto the planet's atmosphere via auroral emissions; this has been observed from X-rays to radio wavelengths with ground- and space-based telescopes. Jupiter has the advantage for us over the rest of the outer planets of not just being very large but also being much closer, allowing high-quality measurements to be made from Earth.

The magnetosphere of Jupiter extends well beyond the orbits of the Galilean satellite system (► [Fig. 6-4](#)), and it is these moons that provide much of the plasma (► [Table 6-3](#)) and some interesting magnetospheric phenomena. In particular, Io loses about 1 ton/s of atmospheric material (mostly SO_2 and dissociation products), which, when ionized to sulfur and oxygen ions, becomes trapped in Jupiter's magnetic field (► [Fig. 6-12](#)). Coupling to Jupiter causes the magnetospheric plasma to corotate with the planet. Strong centrifugal forces confine the plasma toward the equator. Thus, the densest plasma forms a torus around Jupiter at the orbit of Io.

Compared with the local plasma, which is corotating with Jupiter at 74 km/s, the neutral atoms are moving slowly, close to Io's orbital speed of 17 km/s. When a neutral atom becomes ionized (via electron impact), it experiences an electric field, resulting in a gyromotion of 57 km/s. Thus, new S^+ and O^+ ions gain 540 and 270 eV in gyro-energy. The new "pickup" ion is also accelerated up to the speed of the surrounding plasma. The necessary momentum comes from the torus plasma, which is in turn coupled, via field-aligned currents, to Jupiter – the jovian flywheel being the ultimate source of momentum and energy for most processes in the magnetosphere. About one-third to one-half of the neutral atoms are ionized to produce additional fresh plasma, while the rest are lost via reactions in which a neutral atom exchanges an electron with a torus ion. On becoming neutralized, the particle is no longer confined by the magnetic field and flies off as an energetic neutral atom. This charge-exchange process adds gyro-energy to the ions and extracts momentum from the surrounding plasma, but it does not add more plasma to the system.



■ Fig. 6-12

The main components of the Jupiter-Io system

The Io plasma torus has a total mass of ~ 2 megaton, which would be replenished by a source of ~ 1 ton/s in ~ 23 days. Multiplying by a typical energy ($T_i \sim 60$ eV, $T_e \sim 5$ eV), we obtain $\sim 6 \times 10^{17}$ J for the total thermal energy of the torus. The observed UV power is about 1.5 TW, emitted via more than 50 ion spectral lines, most of which are in the EUV. This emission would drain all the energy of the torus electrons in ~ 7 h. Ion pickup replenishes energy, and Coulomb collisions feed the energy from ions to electrons but not at a sufficient rate to maintain the observed emissions. A source of additional energy, perhaps mediated via plasma waves, seems to be supplying hot electrons and a comparable amount of energy as ion pickup. The 20–80 day time scale (equivalent to 50–200 rotations) for the replacement of the torus indicates surprisingly slow radial transport that maintains a relatively strong radial density gradient. Flux tubes laden with denser, cooler, plasma move outward and relatively empty flux tubes containing hotter plasma from the outer magnetosphere move inward.

Voyager, Galileo, and, particularly, Cassini observations of UV emissions from the torus show temporal variability (by about a factor 2) in torus properties (Steffl et al. 2004, 2006). Models of the physical chemistry of the torus match the observed properties in regard to the production of neutral O and S atoms, a radial transport time, and a source of hot electrons (Delamere and Bagenal 2003). Steffl et al. (2008) showed that a small ($< 1\%$) hot electron population that varies with longitude and drifts by a few percent with respect to corotation could explain modulations in ionization state and emissions. The source of these hot electrons is not understood, but the discussions of what processes might be causing periodicities observed at Saturn (see next section) suggest that perhaps ionospheric winds might be driving currents through the jovian magnetosphere, carried by these hot electrons. On longer time scales, the

variation in torus emissions observed over several months by Cassini reflect the observed changes in the output of Io's volcanic plumes (Delamere et al. 2004; Bagenal and Delamere 2011).

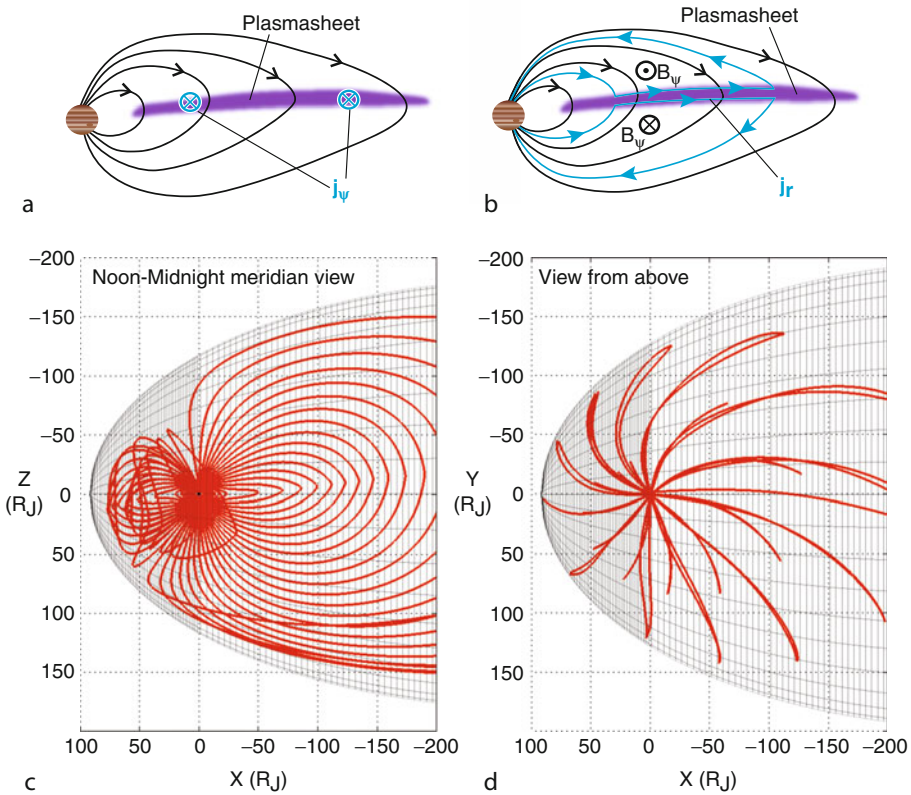
The earliest theoretical studies concluded that the magnetosphere of Jupiter is “all plasma-sphere” with little influence of solar-wind-driven convection. Indeed, rotation dominates the plasma flows observed in the jovian magnetosphere out to distances $\sim 70 R_J$. Yet, the presence of sulfur and oxygen ions in the middle magnetosphere, far from Io, indicates that plasma is transported outward, in directions transverse to the magnetic field.

The net radial transport is thought to be slowest near Io's orbit (~ 15 m/s) and to speed up farther out (~ 50 m/s beyond $10 R_J$). Plasma from the Io torus spreads out from Jupiter as a $\sim 5 R_J$ -thick plasma sheet throughout the magnetosphere. While the flow direction remains primarily rotational, both a lag behind corotation and local time asymmetries increase steadily with distance from the planet. Bursts of flow down the magnetotail are observed and also, on the dawn flanks, occasional strong bursts of super-rotation. Below we return to these deviations from corotation and discuss how they relate to auroral structures.

As the equatorial plasma rotates rapidly, it exerts a radial (centrifugal) stress on the flux tubes. Additional stress is provided by the radial pressure gradient of the plasma, inflating the magnetic field (see [Fig. 6-13](#)). The net result is a stretching of the initially dipolar field lines away from the planet, in a configuration that implies an azimuthal current in the near-equatorial disk ([Fig. 6-13a](#)). The lower two panels of [Fig. 6-13](#) show magnetic field lines derived from models that include the internally generated field plus the effects of currents on the magnetopause and in the plasma sheet. [Figure 6-8d](#) shows magnetic field lines projected onto the equatorial plane and illustrates how the field lines also bend or “curl” in the azimuthal direction, which means that there are also radial currents in the equatorial plasma sheet ([Fig. 6-13b](#)). Alternatively one can think of sub-corotating plasma pulling the magnetic field away from radial. At Jupiter, the field is more or less azimuthally symmetric out to about $50 R_J$, but [Fig. 6-13d](#) shows that strong local time asymmetries develop in the outer magnetosphere (Khurana 2001; Khurana and Schwarzl 2005).

Just as at Earth, the auroral emissions at Jupiter are important indicators of magnetospheric processes. With limited spacecraft coverage of these magnetospheres, auroral activity is a projection of magnetospheric processes, communicated via precipitating energetic particles, onto the atmosphere; thus, it allows us to study global processes not yet accessed by spacecraft. [Figure 6-14](#) illustrates the three main types of aurora at Jupiter (see the reviews by Bhardwaj and Gladstone 2000; Clarke et al. 2005). There is a fairly steady main auroral oval that produces approximately 10^{14} W globally and that can exceed 1 W m^{-2} locally. This oval is quite narrow, corresponding to about 1° in latitude or a few hundred kilometers horizontally in the atmosphere of Jupiter and mapping along magnetic field lines to $(20\text{--}30)R_J$ at the equator in the magnetosphere, well inside the magnetopause. Auroral emissions are also observed at the feet of flux tubes at Io, Europa, and Ganymede. While the magnetosphere interaction with Callisto is thought to be much weaker than for the other satellites, any Callisto aurora would be difficult to separate from the main aurora. The Io-related aurora includes a “wake” signature that extends halfway around Jupiter. The third type of jovian aurora is the highly variable polar aurora, which occurs at higher latitudes than the main aurora, corresponding to greater magnetospheric distances.

The fact that the shape of the jovian main auroral oval is constant and fixed, in magnetic coordinates (including an indication of a persistent magnetic anomaly in the northern hemisphere), tells us that the auroral emissions correspond to a persistent magnetospheric process

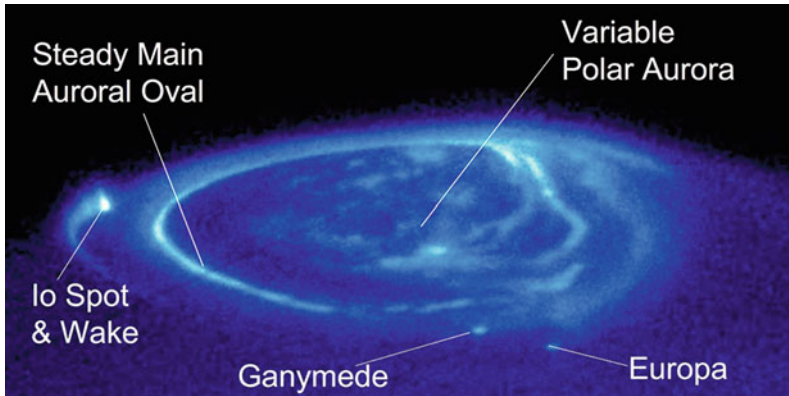


■ Fig. 6-13

Magnetic field configuration and current systems in Jupiter's magnetosphere. The top diagrams show the (a) azimuthal and (b) radial current systems. The lower diagrams show the magnetic field configuration (c) in the noon-midnight meridian plane and (d) in the equatorial plane derived from in situ magnetic field measurements (Khurana and Schwarzl 2005)

that causes a more or less constant bombardment of electrons onto Jupiter's atmosphere. Unlike the terrestrial auroral oval, the jovian oval has no relation to the boundary between open and closed field lines of the polar cap; it maps to regions well within the magnetosphere. It is difficult to map the magnetic field lines accurately because of the strong equatorial currents, which are variable and imprecisely determined. But it has become clear that the main aurora is the signature of Jupiter's attempt to spin up its magnetosphere or, more accurately, Jupiter's failure to spin up its magnetosphere fully.

● Figure 6-8a shows the simple current system proposed by Hill (1979). As the Io-genic plasma moves outward, the conservation of angular momentum would suggest that the plasma should lose angular speed. In a magnetized plasma, however, electrical currents easily flow along magnetic fields and couple the magnetospheric plasma to Jupiter's flywheel. Hill (1979) argued that at some point the load on the ionosphere increases to the point where the coupling between the ionosphere and corotating atmosphere – manifested as the ionospheric conductivity – is not sufficient to carry the necessary current, causing the plasma to lag behind corotation. Using a



■ Fig. 6-14

Three main regions of Jupiter's aurora: Main oval, satellite footprints, polar emission (From Clarke et al. 2005)

simple dipole magnetic field, Hill (1979) obtained an expression for the critical distance for corotation lag that depended on the mass production and transport from Io and the (poorly determined) ionospheric conductivity. Matching his simple model to the Voyager observations of McNutt et al. (1979) and Hill et al. (1981) found he could model the observed profiles of azimuthal flow with a source giving 2–5 ton/s and an ionospheric conductivity equal to 0.1 mho. Over the past decade, Jupiter's main aurora has become an active area of study. Researchers have considered the effects of the non-dipolar nature of the magnetic field, the narrowness of the auroral emissions, realistic mass-loading rates, the nonlinear feedback of ionospheric conductivity responding to electron precipitation, and the development of electrostatic potential drops in the region of low density between the ionosphere and torus (Cowley and Bunce 2001, 2003; Nichols and Cowley 2005; Ray et al. 2010). The understanding of plasma processes developed in the terrestrial magnetosphere is being applied to the different regimes at Jupiter and will ultimately be tested when the Juno spacecraft goes into a close polar orbit in 2016.

The auroral emissions poleward of the main auroral oval (see ● Fig. 6-14) are highly variable; they are modulated by the solar wind and controlled in local time, being usually dark on the dawn side and brighter on the dusk side (see the reviews by Grodent et al. 2003; Clarke et al. 2005). The region of magnetic field lines that is open to the solar wind in the polar cap is thought to be relatively small (Vogt et al. 2011). Thus, much polar auroral activity reflects activity in the outer magnetosphere, occurring on closed magnetic field lines. Polar auroral activity has been associated with polar cusps (Waite et al. 2001; Pallier and Prangé 2004; Bunce et al. 2004) as well as tail plasma sheet reconnection and the ejection of plasmoids down the magnetotail (Grodent et al. 2004; Radioti et al. 2008, 2010, 2011; Ge et al. 2010). Spectral observations of auroral X-ray flares suggest that energetic ions are bombarding the polar atmosphere and may be the signature of the plasma sheet return (downward) current (Waite et al. 1994; Cravens et al. 1995; Hui et al. 2010; Ozak et al. 2010).

A major interest in studying the aurora is to explore how the various emissions are related to the dynamics of the outer magnetosphere. The innermost region, which we will call the Hill region, comprises the equatorial plasma disk where rotation dominates the flow. At a distance

of about $20 R_J$, the lag of plasma in the equatorial plasma sheet behind strict corotation drives upward currents, and the associated electron bombardment of the atmosphere causes the main aurora.

The middle magnetosphere is a compressible region (sometimes called the “cushion” or Vasyliunas region, after his seminal article (Vasyliunas 1983) in which the dynamics of the outer magnetosphere was first addressed in a substantial fashion). On the dayside of the magnetosphere, the ram pressure of the solar wind compresses the magnetosphere. Inward motion on the dawn side reduces the load on the ionosphere, producing a correspondingly dark region in the dawn polar aurora (🔗 Fig. 6-14). On the dusk side, the plasma expands outward and strong currents try to keep the magnetospheric plasma corotating. These strong currents produce the active dusk polar aurora. Kivelson and Southwood (2005) argued that the rapid expansion of flux tubes in the afternoon to dusk sector means that the second adiabatic invariant is not conserved, which results in the heating and thickening of the plasma sheet.

Pursuing evidence for Vasyliunas’ argument that plasmoids are ejected down the jovian magnetotail, Grodent et al. (2004) found evidence of spots of auroral emission poleward of the main aurora connected to the nightside magnetosphere that flashed with an approximately 10-min duration. Such events were rare, recurring only about once per 1–2 days. These flashes seemed to occur in the pre-midnight sector, and Grodent et al. (2004) estimated that they are coupled to a region of the magnetotail that was about $5R_J$ – $50R_J$ across and located further than $100R_J$ down the tail. Studies of in situ measurements (Russell et al. 2000; Woch et al. 2002; Vogt et al. 2010; Ge et al. 2010) led to the conclusion that plasmoids on the order of $\sim 25R_J$ in scale were being ejected every 4 h–3 days, with a predominance for the post-midnight sector and distances of 70– $120R_J$. Could such plasmoids account for most of the plasma loss down the magnetotail? Bagenal (2007) approximated a plasmoid as a disk of plasma sheet $2R_J$ thick having diameter $25R_J$ and density of 0.01 cm^{-3} , so that each plasmoid has a mass of about 500 ton. Ejecting one such plasmoid per day is equivalent to losing 0.006 ton/s. Increasing the frequency to once per hour raises the loss rate to 0.15 ton/s. Thus, on the one hand, even with optimistic numbers, the loss of plasma from the magnetosphere due to such plasmoid ejections cannot match the canonical plasma production rate, 0.5 ton/s. On the other hand, a steady flow of plasma of density 0.01 cm^{-3} , in a conduit that is $5R_J$ thick and $100R_J$ wide, moving at a speed of 200 km/s would provide a loss of 0.5 ton/s. Such numbers suggest that a quasi-steady loss rate is feasible. The question of the mechanism remains unanswered. Bagenal (2007) proposed three options: a diffusive “drizzle” across weak, highly stretched, magnetotail fields; a quasi-steady reconnection of small plasmoids, below the scale detectable via auroral emissions; or a continuous but perhaps gusty magnetospheric wind.

In the spring of 2007, the New Horizons spacecraft flew past Jupiter, getting a gravitational boost on its way to Pluto, and made an unprecedented passage down the core of the jovian magnetotail, exiting on the northern dusk flank. For over 3 months, while covering a distance of $2,000R_J$, the spacecraft measured a combination of iogenic ions and ionospheric plasma (indicated by H^+ and H^{3+} ions) flowing down the tail (McComas et al. 2007; McNutt et al. 2007). The fluxes of both thermal and energetic particles were highly variable on time scales of minutes to days. The tailward fluxes of internally generated plasma led (McComas and Bagenal 2007) to argue that perhaps Jupiter does not have a complete Dungey cycle but that the large time scale for any reconnection flow (see 🔗 Table 6-4) suggests that magnetic flux that is opened near the subsolar magnetopause re-closes on the magnetopause before it has traveled down the tail. They suggested that the magnetotail comprises a pipe of internally generated plasma that disconnects from the planetary field and flows away from Jupiter in intermittent surges or bubbles,

with no planetward Dungey return flow. Delamere and Bagenal (2010) argue that, due to the viscous processes on the magnetopause boundary, along the flanks of the magnetotail, solar wind plasma becomes entrained and mixed with the ejected iogenic material.

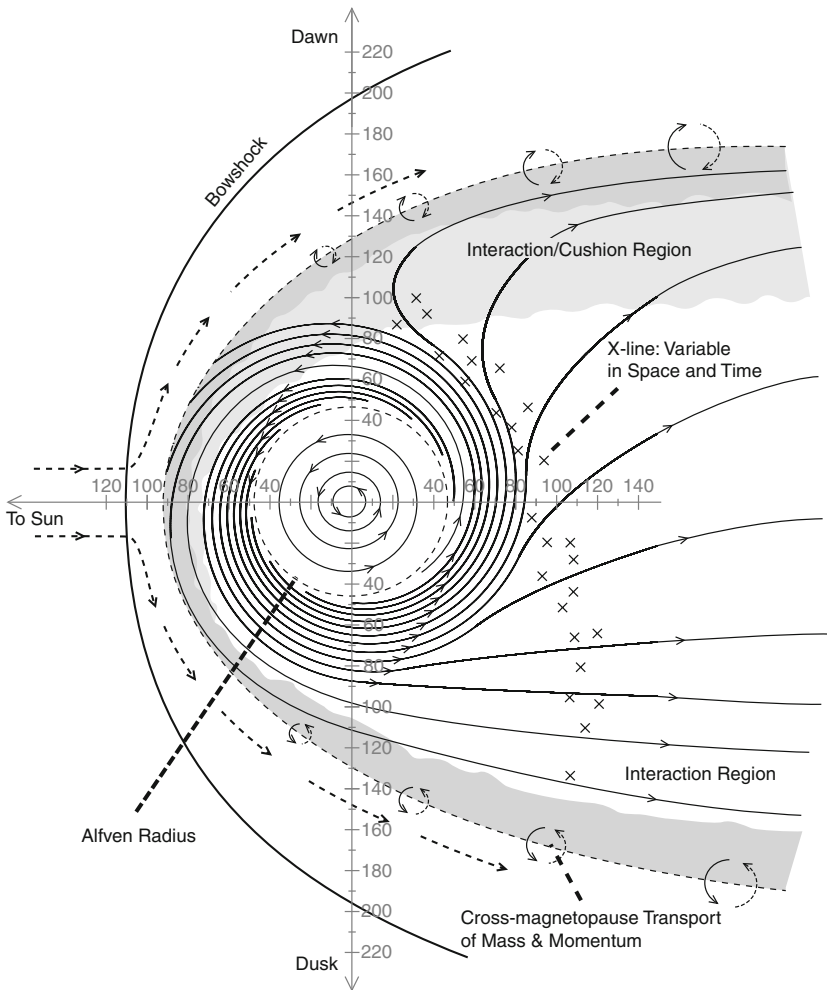
An overview sketch of the dynamics of the magnetosphere as proposed by Delamere and Bagenal (2010) is presented in [Fig. 6-15](#). Alternative views combine the Vasyliunas rotationally driven ejection of plasmoids of [Fig. 6-11](#) with the Dungey cycle of [Fig. 6-9](#) (e.g., Cowley et al. 2007, 2008b; Kivelson and Southwood 2005). Hopefully, observations by the Juno mission will distinguish between these different ideas.

3.2 Saturn

Before the Cassini mission, it was tempting to dismiss the magnetosphere of Saturn as merely a smaller, less exciting, version of the jovian magnetosphere. However, Cassini measurements of the particles and fields in Saturn's neighborhood have shown processes similar to those at Jupiter (e.g., satellite sources, ion pickup, flux tube interchange, corotation, etc.), but they have also revealed substantial intriguing differences (for reviews of initial results of the Cassini mission see Dougherty et al. 2009). The magnetosphere of Saturn is strongly dominated by neutral atoms and molecules. The number-density ratio of neutrals to ions is 12:1 in the Enceladus torus compared with 1:20 in the Io torus. In contrast with Jupiter's steady main aurora, Saturn's auroral emissions are strongly modulated by the solar wind, particularly the solar wind ram pressure. While one might expect the alignment of Saturn's magnetic axis with the planet's spin axis to produce an azimuthally symmetric magnetosphere, observations show an intriguing rotational modulation. Even more mysteriously, the rotational modulation varies with time (on time scale of \sim years) and is different for the northern and southern hemispheres. The magnetosphere of Saturn is shown in [Fig. 6-16](#). Below, we provide a brief summary of current ideas about these topics, which are under active research as the Cassini spacecraft continues to orbit Saturn.

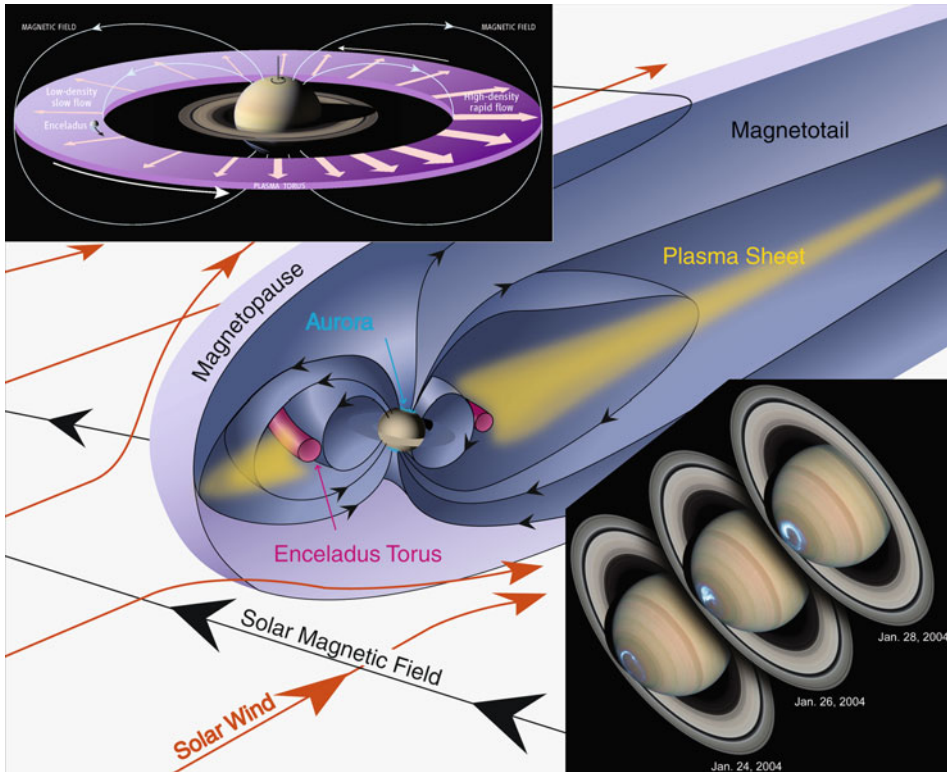
One of the great discoveries of the Cassini mission to Saturn has been the active volcanism of the small icy moon Enceladus. While Enceladus is a mere one-seventh the size of Io, this small moon suffers tidal heating that drives the eruption of geysers from the south polar region. The geyser plumes, extending over 500 km from the surface, seem to be mostly ice particles with water vapor and minor quantities of molecular nitrogen, methane, and carbon dioxide (Porco et al. 2006; Hansen et al. 2006; Waite et al. 2006).

Estimates of the total neutral production rate of water molecules (presumably ultimately coming from Enceladus' plumes) vary around the initial value of 300 kg/s, determined from the initial UV occultation of the plume by Hansen et al. (2006) which is the same as from the earlier (Jurac and Richardson 2005) model constructed to match HST observations of the OH neutral cloud. Sittler et al. (2008) preferred 600 kg/s but only claimed a factor of 2 accuracy, so this value is still consistent with Hansen et al. (2006)'s 300 kg/s. Saur et al. (2008) modeled the electrodynamics of the plume deriving values as high as 1,600 kg/s for the E0 flyby and as low as 200 kg/s for E1 and E2. Meanwhile, a value of \sim 200 kg/s was derived from a second UV occultation reported by Hansen et al. (2008). Similarly, Fleshman et al. (2010a, b) found 100–180 kg/s was consistent with their physical chemical modeling of the Enceladus torus. Finally, Smith et al. (2010) have analyzed INMS data from three Cassini flybys of Enceladus from which they conclude that the net production has increased from <72 kg/s (at the time of E2) to 190 kg/s (at E3) to 750 kg/s (at E5). Thus, the Enceladus neutral source rate could have varied by a factor of 10 between July 2005 and October 2008.



■ Fig. 6-15

Composite sketch of the structure and dynamics of the jovian magnetosphere. Inside $\sim 60 R_J$ the plasma flow is corotational and the plasma sheet has little local time asymmetry. Beyond $\sim 60 R_J$, radial outflow combines with rotation to produce spiral flow that removes the plasma from the magnetosphere within about a day. Beyond $\sim 80\text{--}100 R_J$, blobs of plasma detach (at an x point) and are shed down the magnetotail. Between midnight and dawn the region of x-points is well defined by in situ observations and is consistent with estimates of the location where tailward Maxwell stresses dominate over confinement by the planetary magnetic field. In the dusk to premidnight region the location of x points is not well determined, but observational evidence suggests that it could be as far as $150\text{--}200 R_J$ downtail. Strong velocity shear across the magnetopause drives instabilities that act as a viscous-like interaction between the draped solar wind and largely closed magnetosphere, intermittently transferring mass and momentum across the magnetopause boundary. This interaction region is particularly wide on the dawnside of the magnetosphere, corresponding to what is sometimes called the “cushion region”. After Delamere & Bagenal (2011)



■ Fig. 6-16

Center: Three-dimensional schematic representation of the magnetosphere of Saturn. **Top left:** Sketch of asymmetric plasma disk where Gurnett et al. (2007) propose that the observed density variations are caused by a pattern of asymmetric radial outflows. **Bottom right:** Hubble Space Telescope observations of Saturn's auroral emissions (Clarke et al. 2005)

The fate of the neutrals is more complicated at Saturn than Jupiter. The high neutral-to-ion density ratio at Saturn is a result of lower ionization rates (caused as much by photoionization at Saturn as electron-impact ionization that dominates at Jupiter). Only a fraction of the neutral material is transported out into the plasma sheet. Some of the corotating ions charge exchange with neutrals to become escaping fast neutrals but other collisional processes such as photo- and electron-dissociation, neutral–neutral collisions, and low-velocity charge exchange “puff” up the neutral cloud, spreading it beyond Enceladus’ orbit ($4R_S$) as well as sending a substantial flux of neutrals into the planet Saturn.

It is not clear that the rate of ionization vs. other neutral loss processes would be maintained at the modeled fractions if the neutral source increases to Smith et al. (2010)’s E5 values of ~ 750 kg/s or Saur et al. (2008)’s E0 value of 1,600 kg/s. Neutral production increases the amount of neutral–neutral collisions that would cause more of the material to spread out from Enceladus’ orbit. One might expect that more material would escape as neutrals rather than be ionized. Electron-impact ionization would be reduced due to collisional cooling of the electrons. In fact, Tokar et al. (2009) do not report higher-than-average plasma densities around

the time of E5. Estimates of the plasma source range between 12 and 250 kg/s (see review by Bagenal and Delamere 2011).

The nearly three orders of magnitude difference in the ion–neutral density ratios of the two magnetospheres can be explained in terms of a much lower energy input into the Saturn system (Delamere et al. 2007). At Saturn, the plasma flowing past Enceladus (at an orbital distance of ~ 4 saturnian radii) has a slower speed than the plasma flow past Io (at ~ 6 jovian radii). A factor 2 difference in relative motion (i.e., 26 km/s at Enceladus as against 57 km/s at Io) means that new ions pick up a factor 4 less energy. With less pickup energy, the ions deliver less energy to the electrons. At low electron temperatures, the ionization rates plummet and, correspondingly, plasma production drops. In fact, Delamere et al. (2007) showed (backed up by an extensive study by Fleshman et al. 2010a, b) that without an additional source of hot electrons (similar to that in the Io plasma torus), the Enceladus plasma torus would not be sustained.

The weaker plasma source at Saturn results in weaker centrifugal stresses and weaker magnetospheric currents. Thus, the field structure at Saturn is similar to that shown in  Fig. 6-13 for Jupiter but with less pronounced distortion from dipolar. The plasma pressure is also much reduced, so that Saturn's magnetosphere is less compressible than Jupiter's and shows a less dramatic response to changes in solar wind dynamic pressure (Kanani et al. 2010).

 Figure 6-16 shows Hubble Space Telescope (HST) images of Saturn's aurora (Clarke et al. 2005). In contrast with Jupiter's large main auroral oval, which maps to regions deep inside the magnetosphere, Saturn's small auroral oval and strong variations in auroral intensity with solar wind conditions indicates that Saturn's aurora, like Earth's, marks the boundary of open and closed regions of magnetic flux. The picture was clarified during a campaign of combined Hubble and Cassini observations as the spacecraft approached Saturn in late 2000. For 22 days, Cassini's instruments measured the magnetic field, plasma density, and plasma velocity in the solar wind, while Hubble cameras and the Cassini radio antennas monitored Saturn's auroral activity. Nature cooperated and provided a couple of interplanetary shock waves that passed the Cassini spacecraft on January 15 and 25, 2001, and then hit the magnetosphere of Saturn some 17 h later. Clarke et al. (2005) reported HST observations of the subsequent brightening of auroral emission, and Kurth et al. (2005) reported accompanying increases in radio emission. Crary et al. (2005) show a correlation of auroral intensity with solar wind dynamical pressure, supporting the view that the solar wind has an Earth like role at Saturn.

But further study showed that it was compression of the magnetopause by the solar wind that correlates with auroral intensity rather than reconnection of the solar and planetary magnetic fields. Crary et al. (2005) pointed out that, at Saturn's orbit, the solar magnetic field is essentially tangential so that the solar and planetary fields are largely orthogonal to each other: far from optimal conditions for magnetic reconnection. Clarke et al. (2005, 2009) showed that the brightest auroral emissions occurred after the passage of a solar wind pressure pulse. Cowley et al. (2005) suggested that the rapid compression of Saturn's magnetosphere induces enhanced tail reconnection, which would explain the subsequent shrinking of the auroral oval (see  Fig. 6-9). The explanation for why Saturn's aurora responds to compression rather than the direction of the IMF (as at Earth) principally involves the longer time scale for the solar wind to flow past the larger magnetosphere. Fluctuations of B_z component of the IMF are similar at Earth and Saturn (~ 10 s min to an hour or two). Similarly, the rate of dayside reconnection is thought to be about the same at each planet. But the amount of open flux in Saturn's tail is thought to be much larger than Earth's (about a factor of ~ 100) so the buildup of open flux in the magnetotail (stages 1–4 in  Fig. 6-9) could be much longer, typically ~ 1 week instead of ~ 1 h. So, Saturn's tail will almost never respond to individual intervals of positive B_z , but

instead inflates on time scales comparable to the time between recurrent solar wind pressure pulses. Thus, compression-induced tail reconnection, while rather rare at Earth, may be the usual mode at Saturn (Jackman et al. 2005; Badman et al. 2005).

The magnetospheric processes driving Saturn's aurora began to be better understood after Cassini moved to higher magnetic latitudes in 2007. Observations by Cassini particle and field instruments show a large-scale field-aligned current present at the open–closed field line boundary (Cowley et al. 2008a; Bunce et al. 2008, 2010; Talboys et al. 2009a, b), in the same region as auroral radio emissions were generated (Lamy et al. 2009, 2010).

In the mean time, the difficulties in measuring Saturn's rotation rate have wreaked havoc with our simple ideas of magnetospheric dynamics. So how could one establish how fast the interior of a gas planet is spinning? The usual trick is to measure the periodicity of radio emissions modulated by the planet's internal magnetic field. In this method, it is assumed that the magnetic field is tilted and that the dynamo region where the field is generated spins at a rate representative of the bulk of the planet. Recent Cassini data indicate that apparent changes in Saturn's spin could in fact be caused by processes external to the planet. This raises new questions about how we measure and understand the rotation of the large gas planets. Saturn at first dumbfounded planetary theorists who study dynamo models by being observed to have a highly symmetric internal magnetic field. A field that is symmetric about the rotation axis violates a basic theorem of magnetic dynamos (Cowling 1933). The second puzzle came with the detection of a systematic rotational modulation of the radio emission similar to a flashing strobe, which should not occur for a symmetric magnetic field. Meanwhile, radio measurements have revealed that Saturn's day appears to have become about 6–8 min longer – it is now roughly 10 h and 47 min – since the 1980s when measured by the Voyager missions (Kurth et al. 2008). Furthermore, the spin rate seems to keep changing and may be modulated by the solar wind speed (Zarka et al. 2007) and is different in the northern and southern hemispheres (Gurnett et al. 2009), the rotation rates switching hemispheres over equinox (Gurnett et al. 2010; Southwood 2011). Auroral UV emissions are also modulated at the same rate as the radio emissions (Nichols et al. 2010), as are oscillations in the magnetic fields (Andrews et al. 2010a, b). The variation in modulation with season evokes an atmospheric driver. To drive periodic modulations with thermospheric winds via currents in the ionosphere will require realistic models of Saturn's ionosphere (Smith 2011; Galand et al. 2011).

A fundamental issue is whether the magnetospheric observations, including the radio emissions, do actually require the magnetic field emanating from the interior of Saturn to be asymmetric. Nearly 30 years ago, Stevenson suggested that strong shear motions in an electrically conducting shell surrounding the dynamo might impose symmetry around the rotational axis (Stevenson 1982). That the rotational modulation of magnetospheric phenomena seems to be fairly constant with radial distance, that dynamic changes occur in the external plasma structures around Saturn, and that there is an apparent modulation by the solar wind speed indicate that an external explanation for Saturn's apparently erratic spin rate seems far more plausible than perturbations in the massive interior of the planet. Yet, localized magnetic anomalies (i.e., high-order multipoles) at high latitudes remain possible and may be affecting the currents that couple the magnetosphere to the planet (Southwood and Kivelson 2007). Gurnett et al. (2007) showed how Saturn's radio emission, the magnetic field measured in the magnetosphere, and the density of the plasma trapped in the magnetic field are all modulated with the same drifting period. They argued that the process that transports plasma radially outward could be stronger on one side of Saturn than the other, as illustrated in the top left of  Fig. 6-16. Gurnett et al. (2007) suggested that this circulation pattern also produces higher plasma densities in the region of stronger outflow and proposed that plasma production stresses the

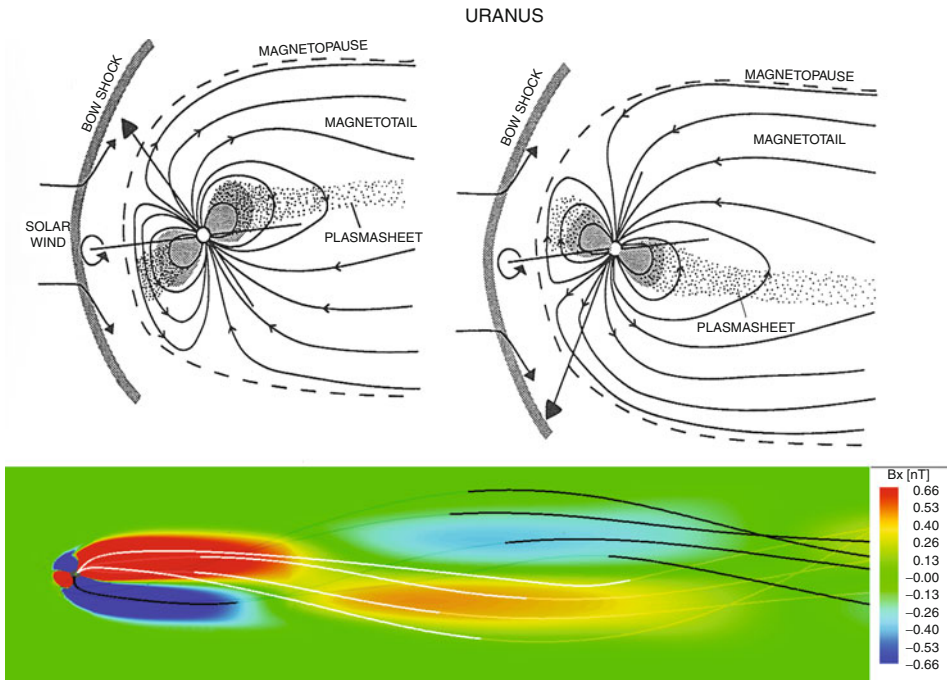
electrodynamic coupling between the magnetosphere and the planet, causing the pattern of weaker or stronger outward flow to slowly slip in phase relative to Saturn's internal rotation. What causes the proposed asymmetric convection pattern? In the 1980s, researchers tried to explain variations in the Io plasma torus (Hill et al. 1981) by invoking a convection pattern that rotated with the planet; however, evidence of such a flow pattern in the jovian magnetosphere remains elusive. Alternatively, a system of neutral winds in Saturn's atmosphere could drag the ionosphere around, which would stir up the magnetosphere electrodynamically and provide a source of hot electrons. Could small variations in the high-energy electron population in the Enceladus torus, similar to those in the Io torus, be causing the dramatic changes in plasma density observed by Cassini? If so, large-scale convection patterns in the magnetosphere may not be necessary, just minor modulations in the electrical currents that flow along the magnetic field between the equatorial plasma disk and the planet's ionosphere, bringing small fluxes of ionizing high-energy electrons to the torus. Delamere and Bagenal (2008) showed that a modulation in the small hot-electron population could produce the factor of 2 variation in plasma density observed by Cassini.

Undoubtedly, the issue of Saturn's rotation rate and its coupling to the magnetosphere will be a vital area of exploration over the next few years. Similarly, it will be important to investigate whether material is ejected down the tail in the manner and to the extent of the jovian system. Only a few plasmoids have been detected to date at Saturn, but this may be a result of limited coverage by the Cassini spacecraft (e.g., Jackman et al. 2008; Hill et al. 2008). The substantial polar cap, marked by the aurora, and the influence of the solar wind on the auroral intensity indicate that the Dungey reconnection cycle plays a substantial role at Saturn. The extent and mechanism whereby any return, planetward, flow operates in the magnetotail awaits further exploration.

3.3 Uranus and Neptune

The Voyager flybys of Uranus (1986) and Neptune (1989) revealed what have to be described as highly irregular magnetospheres. The non-dipolar magnetic fields and the large angle between the magnetic and rotation axes not only pose interesting problems for dynamo theorists but also challenge the ideas of magnetospheric dynamics. Unfortunately, little study has been made of these odd magnetospheres for the past 15 years, and there is only slim hope of further exploration for quite some time. Thus, there is not much to add to the comparative reviews of their fields by Connerney (1993) and of their magnetospheres by Bagenal (1992). Here, we provide a brief précis of these reviews to which the reader should turn for original references.

▶ *Tables 6-1* and ▶ *Table 6-2* as well as ▶ *Fig. 6-4* show Uranus and Neptune to have substantial magnetospheres that envelope most of their satellites. ▶ *Figures 6-2* and ▶ *Fig. 6-3* give a sense of the irregularity of their magnetic fields, approximated as large tilts and offsets. ▶ *Table 6-2* tells us that from just the solar wind and planetary parameters, we should expect both rotation and solar wind coupling to affect the dynamics of these magnetospheres (though the weak IMF of the outer heliosphere suggests that reconnection will be much weaker than at planets closer to the Sun). ▶ *Figures 6-17* and ▶ *6-18* illustrate how the orientations of these planets' magnetic fields (▶ *Fig. 6-2*), which rotate about the planet's spin axis every 16–17 h, might affect the solar wind coupling process. For Uranus around solstice (the Voyager era of the mid-1980s), when the spin axis is pointed roughly toward the Sun, the large tilt of the magnetic axis will result in a magnetosphere that to first approximation resembles that of the

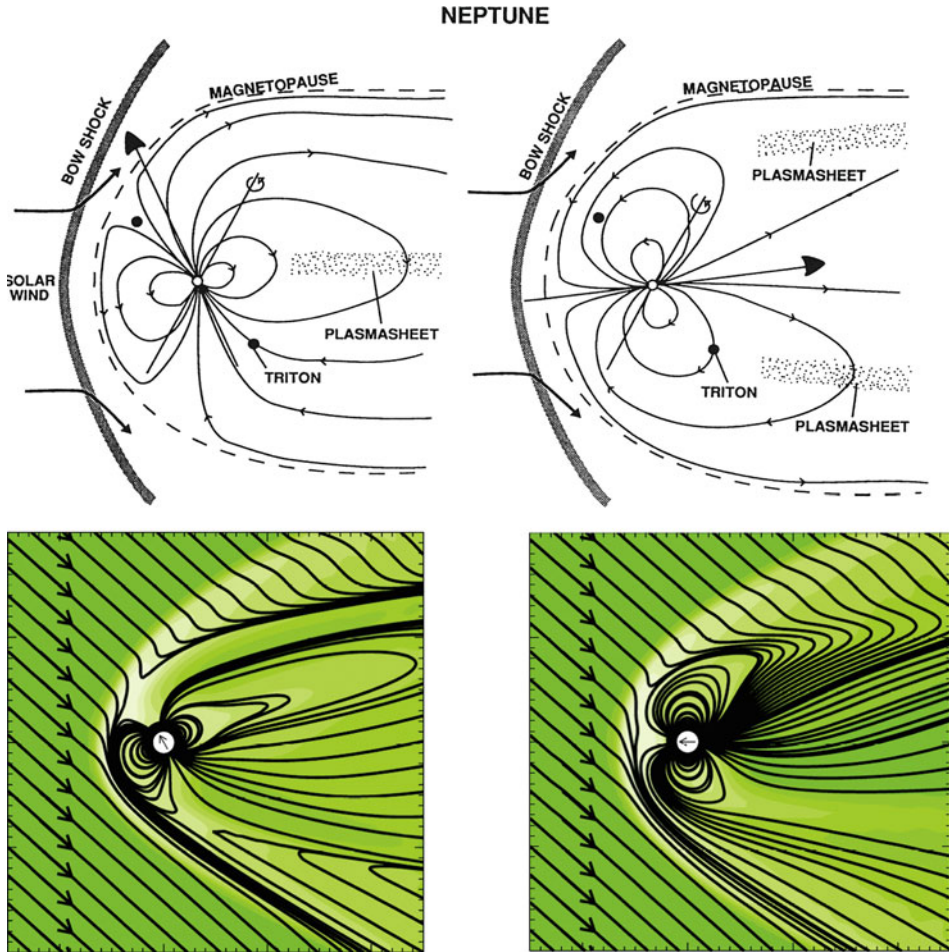


■ Fig. 6-17

The magnetosphere of Uranus at solstice (time of Voyager 2 flyby). The *top left* and *right* sketches show the configuration at different phases of the planet's 18-h spin period (Bagenal 1992). The *bottom panel* shows a numerical simulation of the helical magnetotail (Toth et al. (2004))

Earth but revolves every 17 h. The finite propagation (at the Alfvén speed) of this rotational modulation down the magnetotail produces a helical plasma sheet and braided lobes of oppositely directed magnetic field (► Fig. 6-17). At Neptune, the planet's obliquity being similar to Earth and Saturn, one might have expected the fairly simple configurations of either of those planet's magnetospheres. But the large tilt angle discovered by Voyager results in a configuration that changes dramatically (the tail current sheet changes from a plane to a cylinder) over the 16-h rotation period (► Fig. 6-18).

The large range of the “solar wind angle” (see the last row of ► Table 6-2) indicates that substantial changes in orientation of the planet's spin with respect to the radial direction of the solar wind occur over the (long) orbital periods of these planets. Thus, one has the interesting challenge of imagining how the magnetosphere of Uranus was behaving during equinox in 2007, when the spin axis was perpendicular to the solar wind direction (and parallel or antiparallel to the IMF direction). Unfortunately, we are unlikely to have measurements in the near future to test the output of our imaginations. Such speculations are not wasted, however, since it is quite possible that such configurations – and many others – could have occurred in earlier epochs of Earth's history (as modeled by Zieger et al. 2004) or may now be occurring in any of the giant planets detected in other solar systems. Furthermore, keen young scientists are proposing missions to these water giant planets that might test these ideas in future decades (Arridge et al. 2011).



■ Fig. 6-18

The magnetosphere of Neptune in the configuration corresponding to the time of the Voyager 2 flyby (Bagenal 1992). Over the 19-h spin period the magnetospheric plasma sheet in the tail changes from roughly planar to a cylindrical. From a simulation by Zieger et al. (2004). (Bottom) Diurnal variation of the magnetic field configuration and pressure in an equatorial dipolar magnetosphere for dipole axis at 30° to the normal to the ecliptic plane (left) and at 90° (right). The configurations are close to those relevant to Neptune's magnetosphere at different times during a planetary rotation period

4 Small Magnetospheres

The smallest objects with internal dynamos are Mercury and Ganymede. These mini-magnetospheres were reviewed by Kivelson (2007). The small innermost planet and the solar system's largest moon are about the same size and both are believed to have iron cores. Approximately dipolar magnetic fields have been detected; these hold off the surrounding plasma flow to make small but distinct magnetospheres.

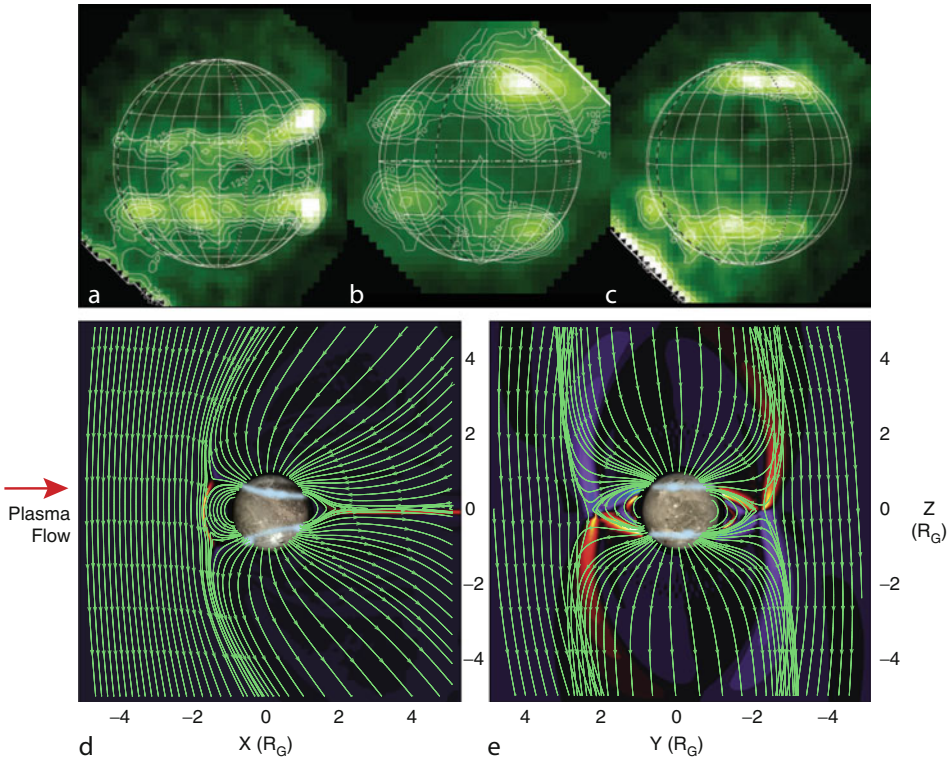
Both Mercury and Ganymede rotate slowly so that neither has a plasmasphere. But in both cases, a significant population of energetic (10s–100s keV) particles have been detected in trapped radiation belts. These energetic particles are likely accelerated in mini-substorms in their magnetotails, but the particles are easily scattered onto the object and probably do not spend more than a few minutes in the magnetospheres. The interaction with these objects with their surroundings is largely between the ambient and dipolar magnetic field. The corresponding time scales for such a Dungey cycle (see [Fig. 6-9](#)) is seconds to minutes in these mini-magnetospheres, rather than minutes to hours at Earth.

4.1 Mercury

Just two brief flybys by Mariner 10 in the early 1970s gave a glimpse of Mercury's magnetosphere (see review by Slavin et al. 2007). These early observations revealed a magnetosphere that, while small, seemed to have most of the main properties observed at Earth ([Fig. 6-5](#)), including a small population of trapped energetic particles, mini-substorms, and particle injections from the magnetotail, basically consistent with simple magnetospheric scaling laws (Slavin et al. 2010). The arrival of the MESSENGER spacecraft in 2011 and the future launch of the Bepi Colombo mission have provoked further thought about this largely forgotten little magnetosphere. Preliminary results from MESSENGER have revealed and the dipole is tilted less than 3° but offset northward by 484 ± 11 km, nearly 20% of the radius (Anderson et al. 2011). The small magnetosphere is very dynamic with dramatic changes occurring on time scales of seconds to minutes (Slavin et al. 2010). Slavin et al. (2009) determined that the rate of reconnection at Mercury's dayside magnetopause to be ~ 10 times that typical at Earth, most probably a result of the low solar wind Alfvén Mach number and values of plasma β (see [Sect. 2.4.3](#)) typical of the inner heliosphere (Slavin and Holzer 1979). The structure and dynamics of the magnetotail resemble the Earth, responding to changes in IMF direction but on shorter time scales and greater intensity, including quasiperiodic ejection of plasmoids down the tail (Slavin et al. 2010). Issues that MESSENGER will address will be how plasma is trapped and accelerated in this tiny magnetosphere, how it responds to the increasing dynamics of the new solar cycle, and how the magnetosphere couples to a planet that has such a tenuous atmosphere/ionosphere.

4.2 Ganymede

Ganymede's magnetosphere sits deep within the magnetosphere of Jupiter (for the background and discussion of Galileo observations see Kivelson et al. 2004). Unlike the supersonic flows of the solar wind, the magnetospheric plasma impinging on Ganymede is subsonic and sub-Alfvénic. There is no upstream bow shock, therefore, and the flowing magnetospheric plasma convects Jupiter's magnetic field, which is roughly antiparallel to that of Ganymede, toward the upstream magnetopause. The net result is a unique magnetospheric configuration with a region near the equator of magnetic flux that closes on the moon and with polar magnetic flux that connects the moon to Jupiter's north and south ionospheres ([Fig. 6-19a, b](#)). A Dungey-style reconnection cycle seems to operate: upstream reconnection opens previously closed flux, convects flux tubes over Ganymede's pole, and re-closes the flux downstream (see [Fig. 6-10](#)).



■ Fig. 6-19

(Top) HST/STIS images of Ganymede's aurora due to electron impact excitation of oxygen at OI 1356 A (M. McGrath, private communication). Contours illustrate variations in brightness. (a) The leading (downstream) hemisphere taken on 23 Dec. 2000. (b) Jupiter-facing hemisphere taken on 30 Nov. 2003. (c) Trailing (upstream) hemisphere taken on 30 Oct. 1998. (Bottom) Numerical model of the magnetosphere of Ganymede, with the satellite and the location of the auroral emissions superimposed (based on Jia et al. 2008). (d) The view looking at the anti-Jupiter side of Ganymede. (e) The view looking in the direction of the plasma flow at the upstream side (orbital trailing side) of Ganymede, with Jupiter to the left. The shaded areas show the regions of currents parallel to the magnetic field

Computer simulations are helpful in visualizing the interaction process (Paty and Winglee 2006; Paty et al. 2008; Jia et al. 2008, 2009, 2010a), but lack of information about the conductivities of Ganymede's tenuous patchy atmosphere and icy surface limit our understanding of the circuit of electrical currents that couple the magnetosphere to the moon. It is clear that electrical currents reach Jupiter, however, because of the strong auroral emissions (► Fig. 6-14) at the Ganymede footprint (Clarke et al. 2002; Grodent et al. 2009). Short-term (few seconds) variability of aurora at Jupiter associated with the magnetic footprint of Ganymede (Grodent et al. 2009) is perhaps associated with bursty reconnection on the upstream side of Ganymede's magnetosphere (Jia et al. 2010a). The local interaction also bombards electrons into Ganymede's atmosphere, exciting auroral emissions (reviewed by McGrath et al. 2004) as shown in ► Fig. 6-19c. The locations of the aurora on Ganymede are consistent with the boundaries

between regions where the magnetic flux tubes connect at both ends to Ganymede and regions where the flux tubes connect to Ganymede on one end and Jupiter at the other.

5 Induced Magnetospheres

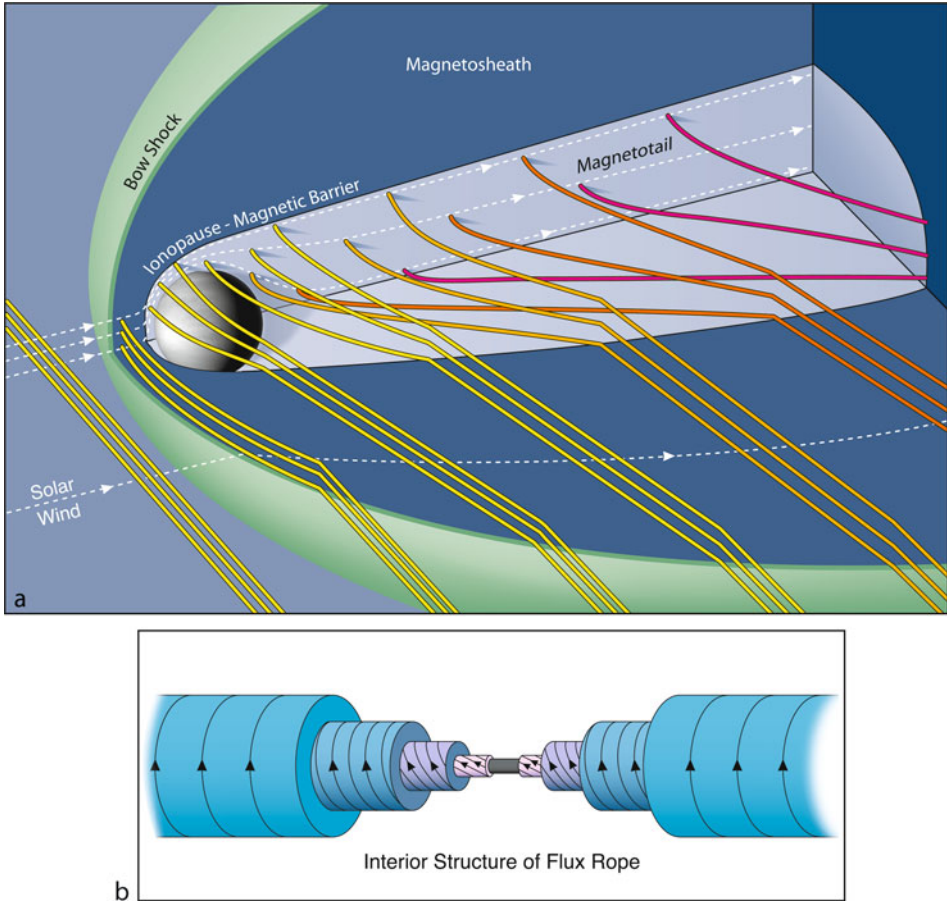
Having discussed the seven objects that have internally generated magnetic fields, we return to the objects without dynamos. The nature of the interaction between such bodies and the plasma in which they are embedded depends on the Mach number of the surrounding flow but is determined principally by the electrical conductivity of the body. If conducting paths exist across the planet's interior or ionosphere, then electric currents flow through the body and into the surrounding plasma, where they create forces that slow and divert the incident flow. In the case of an object sitting in the supersonic solar wind, the flow diverts around a region that is similar to a planetary magnetosphere. Mars and Venus have ionospheres that provide the required conducting paths.

Earth's Moon, with no ionosphere and a very low-conductivity surface, does not deflect the bulk of the solar wind incident on it. Instead, the solar wind runs directly into the surface, where it is absorbed. The absorption leaves the region immediately downstream of the Moon in the flowing plasma (the wake) devoid of plasma, but the void fills in as solar wind plasma flows toward the center of the wake. When the flow impinging on an object is subsonic, no upstream shock forms. But the flow will be absorbed or diverted depending on whether electrical currents flow within the object or within its ionosphere and into the surrounding plasma. Objects interacting with subsonic flow are exemplified by Io; similar processes occur, albeit to a lesser extent, at Enceladus, Titan, Triton, Europa, and several satellites embedded in the giant planet magnetospheres.

5.1 Venus

The magnetic structure surrounding Venus is similar to that around magnetized objects because the interaction causes the magnetic field of the solar wind to drape around the planet (see review by Russell et al. 2006). The draped field stretches out downstream (away from the sun), forming a magnetotail (➤ Fig. 6-20a). The symmetry of the magnetic configuration within such a tail is governed by the orientation of the magnetic field in the incident solar wind, and that orientation changes with time. For example, if the interplanetary magnetic field (IMF) is oriented from east to west, then the symmetry plane (and central current sheet) of the tail is in the north-south direction, and the eastern lobe field points toward the sun while the western lobe field points away from the sun. A west-to-east-oriented IMF would reverse these polarities, and other orientations would produce rotations of the tail's plane of symmetry.

The solar wind brings in magnetic flux tubes that pile up at high altitudes at the dayside ionopause where, depending on the solar wind's dynamic pressure, they may either remain for extended times, thus producing a magnetic barrier that diverts the incident solar wind, or penetrate to low altitudes in localized bundles. Such localized bundles of magnetic flux are often highly twisted structures stretched out along the direction of the magnetic field. Such structures are referred to as *flux ropes*. These flux ropes may be dragged deep into the atmosphere, possibly carrying away significant amounts of atmosphere (➤ Fig. 6-20b).



■ Fig. 6-20

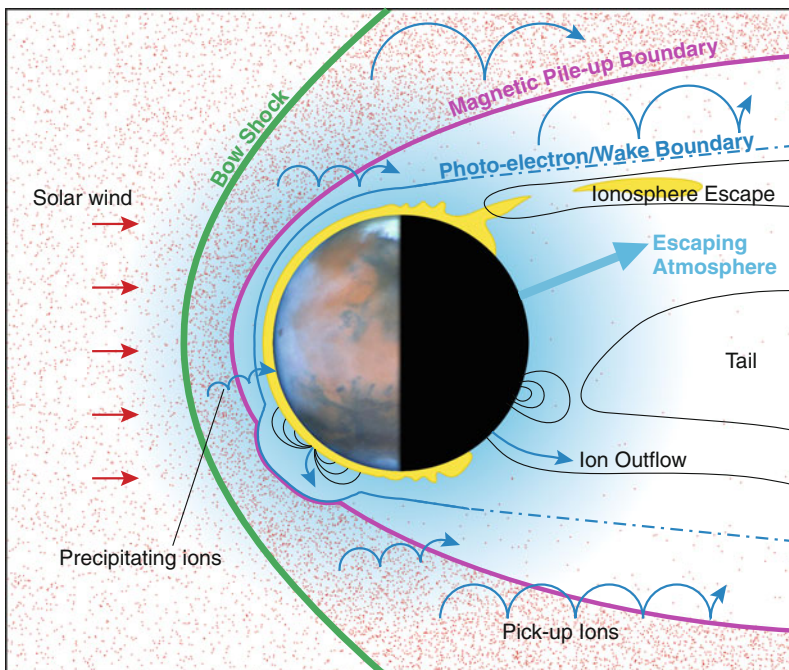
(a) Sketch of the draping of tubes of solar magnetic flux around a conducting ionosphere such as that of Venus. The flux tubes are slowed down and sink into the wake to form a tail (after Saunders and Russell 1986). (b) Schematic illustration of a flux rope, a magnetic structure that has been identified in the ionosphere of Venus. The rope has an axis aligned with the direction of the central field. Radially away from the center, the field wraps around the axis, its helicity increasing with radial distance from the axis of the rope. Structures of this sort are also found in the solar corona and in the magnetotails of magnetized planets

The Venus Express mission has measured the solar wind interaction with Venus revealed some important subtleties. Barabash et al. (2007) report escape of 10^{25} protons/s down Venus' tail. If these ions come from the dissociation and escape of water, then Venus is losing 15 kg/s of water. Delva et al. (2011) use the presence of ion cyclotron waves as evidence of pickup of ionized escaping gases. From analysis of magnetometer data, Zhang et al. (2010) have revealed asymmetries in the magnetotail. By modeling the interaction with a hybrid code (where the electrons are treated as a fluid and the ions as particles), Jarvinen et al. (2010) showed that the large gyroradius of O^+ ions produces an asymmetric tail. Finally, Volwerk et al. (2009, 2010) reports evidence of what could be called substorm activity in Venus' tail.

5.2 Mars

While Mars' remarkably strong remanent magnetism in its crust extends its influence $>1,000$ km from the surface, the overall interaction of the solar wind with Mars is more atmospheric than magnetospheric (see reviews by Nagy et al. 2004 and Brain 2006). Mars interacts with the solar wind principally through currents that link to the ionosphere, but there are portions of the surface over which local magnetic fields block the access of the solar wind to low altitudes (► Fig. 6-21). It has been suggested that “mini-magnetospheres” extending up to 1,000 km form above the regions of intense crustal magnetization in the southern hemisphere; these mini-magnetospheres protect portions of the atmosphere from direct interaction with the solar wind. As a result, the crustal magnetization may have modified the evolution of the atmosphere and may still modify energy deposition into the upper atmosphere.

Several processes involved in the solar wind interaction could have contributed to atmospheric losses at Mars. The outer neutral atmospheres of Venus and Mars extend out into the solar wind where neutral atoms are photoionized and carried away by the solar wind. Newly ionized ions pick up substantial energy and correspondingly large gyroradii. These energetic ions bombard the upper atmosphere, causing heating and ionization. At times of particularly high solar wind pressure, the ionosphere can be stripped away in the solar wind. Fresh ionization in the upstream solar wind also generates plasma waves. The solar wind convects



■ Fig. 6-21

Interaction of the solar wind with the atmosphere, ionosphere, and magnetized crust of Mars illustrating the several processes whereby the planet may have lost much of its atmosphere

the plasma waves toward the planet and into the upper layers of the ionosphere where, funneled and amplified by localized magnetic fields, they heat the ions and drive ion outflows, in a similar way to processes in the polar regions at Earth. Quantitative analyses of these different processes, both currently occurring and in the past, are active areas of research (see Brain et al. 2010 for comparison of different models) and the scientific target of the MAVEN mission to Mars (launch 2013).

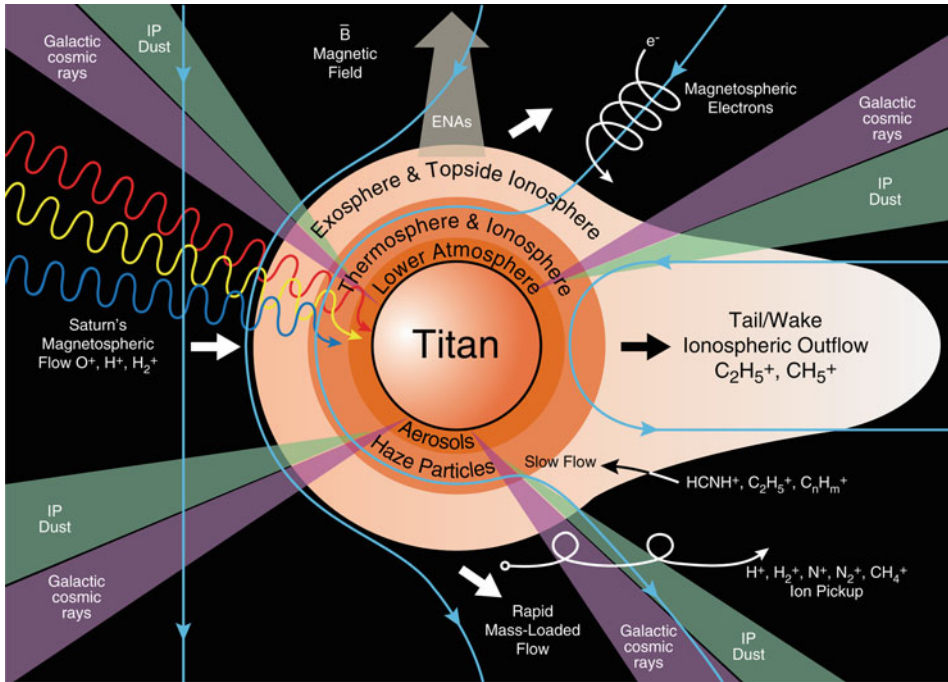
5.3 Titan

With a thick atmosphere and a significant ionosphere, one expects Titan to have an induced magnetosphere similar to that of Venus. Orbiting Saturn at 20 R_S , Titan spends most of the time within the magnetosphere, but when the solar wind compresses the magnetosphere, Titan can spend some of its orbit in the magnetosheath or solar wind. The Voyager 2 flyby in 1980 showed that the magnetospheric plasma was deflected and absorbed, the magnetic field draped around Titan pretty much as expected (see review by Neubauer et al. 1984). The multiple flybys of Titan by the Cassini spacecraft are showing that the situation is more complex, as reviewed by Sittler et al. (2009) and illustrated by the sketch in  Fig. 6-22. There seems to be general agreement that a total of about 300 kg/s of hydrogen is lost from Titan's atmosphere, but estimates of the escape rate of heavier species range from 5 to 85 kg/s (Johnson et al. 2009). The interaction seems to vary significantly with local time and the upstream conditions, and it will require combining the multiple Cassini flybys with models of the interaction before we have a clear consistent picture (Sittler et al. 2009). Nevertheless, it is already clear that the plasma interaction is a significant source of energy as well as a cause of escape for Titan's thick atmosphere (Westlake et al. 2011; Bell et al. 2011).

5.4 Io

The discovery of Io's broad influences on the jovian system predated spacecraft explorations. Bigg (1964) discovered Io's controlling influence over Jupiter's decametric radio emissions. Brown and Chaffee (1974) observed sodium emission from Io, which (Trafton et al. 1974) soon demonstrated to come from extended neutral clouds and not Io itself. Soon thereafter, Kupo et al. (1976) detected emissions from sulfur ions, which Brown (1976) recognized as coming from a dense plasma. With the prediction of volcanism by Peale et al. (1979) just before its discovery by Voyager 1 (Morabito et al. 1979), a consistent picture of Io's role began to emerge. Voyager 1's discovery of Jupiter's aurora and extreme UV emission from the torus (Broadfoot et al. 1979), along with its in situ measurements of the magnetosphere (Bridge et al. 1979), extended our awareness of Io's effect on the larger system.

The ensuing 25 years of observation by interplanetary missions, Earth-orbiting observatories, and ground-based telescopes has deepened our understanding of Io's influences (see the reviews by Thomas et al. 2004 and Schneider and Bagenal 2007). Highlights include Galileo's many close flybys of Io, with detailed fields-and-particle measurements of Io's interaction with the magnetosphere, and Cassini's month-long UV observation of the torus. Progress from Earth-based studies include the Hubble Space Telescope's sensitive UV observations of the footprint aurora and of Io's atmospheric emissions and ground-based observations of new atomic and molecular species in Io's atmosphere and the plasma torus.



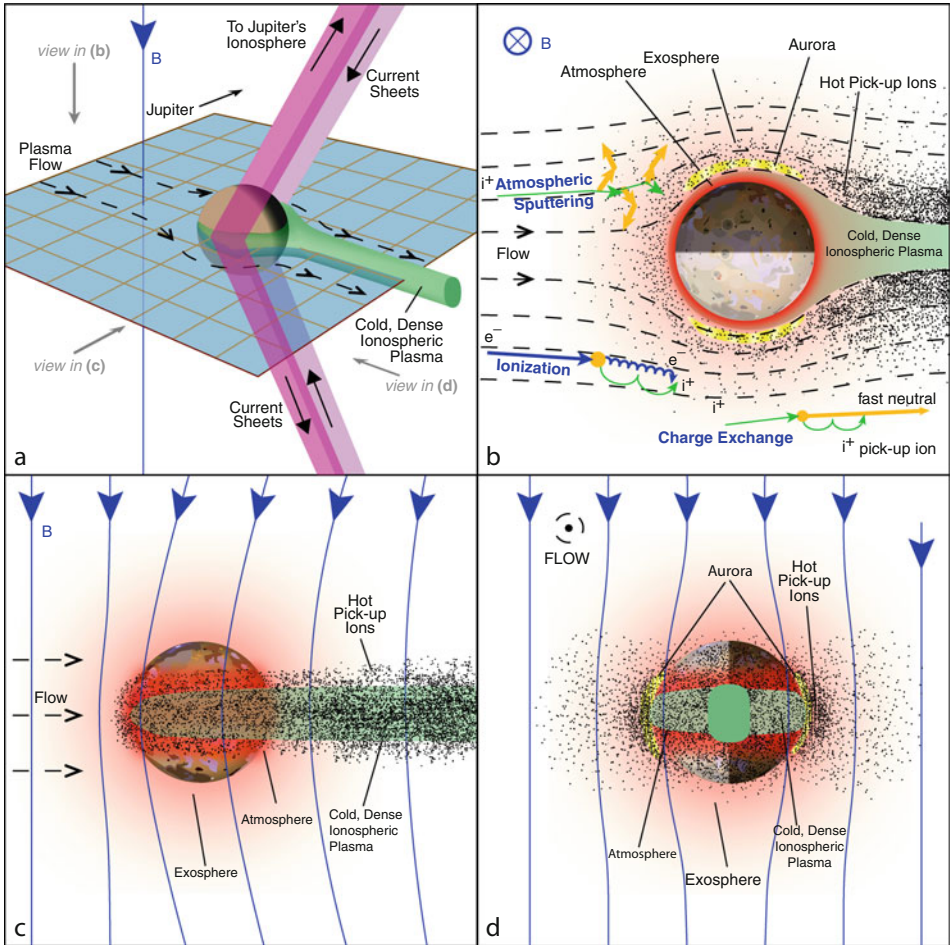
■ Fig. 6-22

Schematic of the processes contributing to source and loss of mass and energy in the plasma interaction with Titan's atmosphere (From Sittler et al. 2009)

Over the age of the solar system, the ton/s loss of Iogenic material to the magnetosphere accumulates to a net decrease in radius of about 2 km. While this loss is significant, Io is not in danger of running out of SO_2 in the lifetime of the solar system. It is plausible, however, that other volatile species such as H_2O were originally present on Io but were completely lost early in its history through processes now depleting Io of SO_2 .

● [Figure 6-23](#) presents a sketch of the interaction of Io with the surrounding plasma that illustrates some of the processes. Inelastic collisions of torus ions with Io's atmosphere heat the atmospheric gases, causing a significant population of neutral molecules and atoms to gain speeds above Io's 2.6 km/s gravitational escape speed. These neutrals form an extensive corona circling most of the way around Jupiter. Io loses about 1–3 tons of neutral atoms per second. How much of the neutral escape is in molecular form (SO_2 , SO, or S_2) as against atomic O or S is not known.

The various ion–electron–atom interactions each have a key effect on the magnetosphere. Most importantly torus ions collide with neutral atoms in the atmosphere, which in turn collide with other atoms in the process known as sputtering. Typically, one torus ion can transfer enough momentum for several atmospheric atoms or molecules to be ejected into Io's corona or possibly to escape from Io altogether. This is the primary pathway for material to be supplied to the neutral clouds and ultimately to the plasma torus. A second key reaction is electron-impact ionization: a torus electron ionizes an atmospheric atom, which is then accelerated



■ Fig. 6-23

Four views of the interaction between Io and the plasma torus. (a) Is a 3-D view showing the current sheets that couple Io and the surrounding plasma to Jupiter's ionosphere. (b) Is a cross-section of the interaction looking down on the north pole of Io, in the plane of Io's equator, when Io is located between the Sun and Jupiter (orbital phase 180, local noon in magnetospheric coordinates). (c) A projected view of the Io interaction looking from the Sun toward Jupiter. (d) A projected view of the interaction from downstream into the flowing plasma (ahead of Io in its orbit)

up to the speed of the plasma and leaves Io. Torus ions can also charge exchange with atmospheric neutrals, which results in a fresh ion and a high-speed neutral. Elastic collisions between ions and atoms can also eject material at speeds between those resulting from sputtering and charge exchange. Finally, electron-impact dissociation breaks down molecules into their component atoms.

► *Figure 6-23* shows that the strong magnetic field of Jupiter affects the interaction in such a way that the flow around Io resembles fluid flow around a cylinder. (Note that a strong intrinsic

magnetic field at Io has been ruled out by Galileo flybys over the poles.) Io's motion through the plasma creates an electrical current. While its surface or interior may be modestly conducting, the current is more likely to be carried in other conducting materials surrounding Io, such as its ionosphere and the plasma produced by ionization of its neutral corona. Currents induced across Io are closed by currents that flow along field lines between Io and Jupiter's polar ionosphere in both hemispheres. Observations by the Voyager 1 and Galileo spacecraft indicate that the net current in each circuit is about 3 million amps. The relative contributions from the conduction current through Io's ionosphere and the current generated by ion pickup in the surrounding plasma remains an issue of debate that awaits more sophisticated models (e.g., see the review by Saur et al. 2004).

A major question regarding Jupiter's magnetosphere is whether most mass loading happens in the near-Io interaction or in the broad neutral clouds far from Io. There is no doubt that substantial pickup occurs near Io, simply owing to the exposure of the upper atmosphere to pickup by the magnetosphere. Pickup near Io is also supported by evidence of fresh pickup ions of molecules (SO_2^+ , SO^+ , S_2^+ , H_2S^+) near Io with dissociation lifetimes of just a few hours. But a closer look shows that the bulk of the Iogenic source comes from the ionization of atomic sulfur and oxygen farther from Io. Galileo measurements of the plasma fluxes downstream of Io suggest that the plasma source from the ionization of material in the immediate vicinity (within $\sim 5R_{\text{Io}}$) of Io is less than 300 kg/s, which is $\sim 15\%$ of the canonical net tons-per-second Iogenic source. The remainder must come from ionization of the extended clouds. It is not clear whether the observations were made during a typical situation, nor it is well established how much the net source and relative contributions of local and distant processes vary with Io's volcanic activity.

While most impacting plasma is diverted to Io's flanks, some is locked to field lines that are carried through Io itself. This $\sim 10\%$ of upstream plasma is rapidly decelerated and moves slowly ($\sim 3\text{--}7$ km/s) over the poles. Most particles are absorbed by the moon or its tenuous polar atmosphere, so that the almost-stagnant polar flux tubes are evacuated of plasma. Downstream of Io, the Galileo instruments detected a small trickle of the cold dense ionospheric plasma that had been stripped away. This cold dense "tail" had a dramatic signature (>10 times the background density), but the nearly stagnant flow (~ 1 km/s) means that the net flux of this cold ionospheric material is at most a few percent of the Iogenic source and quickly couples to the surrounding torus plasma.

The strong electrodynamic interaction generates Alfvén waves that propagate away from Io along the magnetic field (reviewed by Saur et al. 2004). Other MHD modes that propagate perpendicularly to the field dissipate within a short distance. The intense auroral emission in Jupiter's atmosphere at each "foot" of the flux tube (🔗 Fig. 6-14) connected to Io tells us that electrons are accelerated somewhere between Io and the atmosphere. The strong correlation of decametric radio emissions with Io's location also tells us that electrons stream away from Jupiter along the Io flux tube and field lines downstream of Io. But how much of the Alfvén wave energy propagates through the torus and reaches Jupiter is not known. MHD models suggest that much of the wave energy is reflected at the sharp latitudinal gradients of density in the torus. Furthermore, how the Alfvén wave evolves as it moves through the very low-density region between the torus and Jupiter's ionosphere is far from understood. Early ideas suggested that multiple bounces of the Alfvén wave between ionospheres of opposite hemispheres could explain the repetitive bursts of radio emission. More recent studies suggest that the process is more complex, however, with the filamentation of Alfvén waves and the development of quasi-static potential structures (see review by Hess et al. 2010 and references therein).

5.5 Pluto and Comets

Last but not least, there are planetary objects with escaping atmospheres that extend well beyond their solid surface. The neutral atoms and molecules are ionized by solar photons or charge exchange with solar wind protons. The fresh ions are picked up by the solar wind and carried downstream. Momentum is extracted from the solar wind and the IMF that is embedded in the slowed-down flow is stretched out behind the object in a magnetotail, similar to that of Venus shown in [Fig. 6-20](#). The weak solar magnetic field at ~ 30 AU means that the gyro-motions of the newly picked up ions are very large compared to the Pluto system so that a kinetic (or hybrid) approach must be applied in modeling the interaction (see [Delamere 2009](#) and references therein). [Figure 6-24](#) is a sketch of the extended interaction region. The New Horizons spacecraft will fly past Pluto in 2015 and the particle instruments on board ([McComas et al. 2008](#); [McNutt et al. 2008](#)) will determine how close this sketch bears to reality.

6 Outstanding Questions

The tables presented in this chapter quantify the characteristics of the seven magnetospheres of our solar system. The schematics give a glimpse of the diversity of their natures. While magnetospheres must share the same underlying basic physical processes, it is the application to very different conditions at the different planets that makes the study of planetary magnetospheres so interesting and tests our understanding. Below are the major outstanding questions:

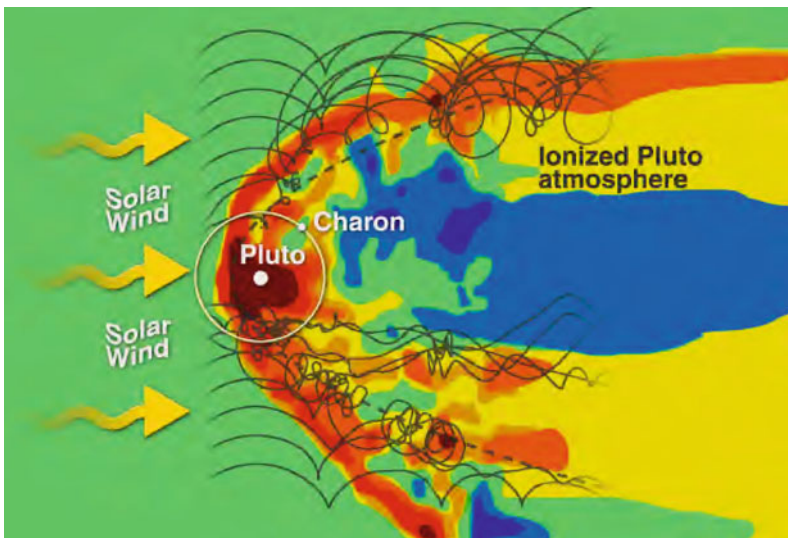


Fig. 6-24

Comet-like interaction of Pluto's escaping atmosphere with the tenuous solar wind at 30 AU. The contours are of ion density. The weak solar magnetic field results in a kinetic process whereby the ions produced by ionization of Pluto's escaping atmosphere exhibit large cycloidal motions, illustrated by sample trajectories in *grey lines*

- How do magnetic dynamos work in the wide range of planetary objects? Why do tiny Mercury and Ganymede have magnetic fields while Earth's sister planet Venus does not? What do the irregular magnetic fields of Uranus and Neptune tell us about their interiors?
- At Saturn, what causes the spin-periodic variability in radio emissions, magnetic field, and plasma properties? What causes the apparent fluctuation in the periodicity?
- How is plasma heated as it moves radially outward in rotation-dominated magnetospheres?
- How is material lost down the magnetotails of Jupiter and Saturn?
- Do Jupiter and/or Saturn have return, planetward, Dungey flows in the magnetotails? If not, how do flux tubes opened by dayside reconnection close and conserve magnetic flux?
- What processes lead to the decoupling of the middle magnetosphere of Jupiter from the planet's rotating ionosphere and cause the narrow auroral oval? What role do parallel potential drops play?
- What processes relate the solar wind variability to the apparent changes in Saturn's main aurora and the polar aurora at Jupiter?
- How do electrical currents couple the magnetospheres of Ganymede and Mercury to these objects with very tenuous atmospheres?
- How are particles accelerated and trapped in the mini-magnetospheres of Ganymede and Mercury?
- What processes have been responsible for removing atmospheric gases (particularly water) over the geological history of Mars and Venus?
- How does the plasma interaction with Titan's atmosphere vary with local time and surrounding plasma conditions? How do these variable conditions affect the fluxes of energy into and material out of Titan's atmosphere?
- What processes are involved in the interactions of Io and Enceladus with their surrounding plasmas? What causes the similarities and differences between the two systems?

References

- Acuña, M. H., et al. 2001, *J. Geophys. Res.*, 106, 23403
- Alexeev, I. I., & Belenkaya, E. S. 2005, *Ann. Geophys.*, 23, 809
- Anderson, B. J., et al. 2010, *Space Sci. Rev.*, 152, 307
- Anderson, B. J., et al. 2011, *Science*, 333, 1859
- Andrews, D. J., Coates, A. J., Cowley, S. W. H., Dougherty, M. K., Lamy, L., Provan, G., & Zarka, P. 2010a, *J. Geophys. Res.*, 115, 12252
- Andrews, D. J., Cowley, S. W. H., Dougherty, M. K., & Provan, G. 2010b, *J. Geophys. Res.*, 115, 4212
- Arridge, C. S., et al. 2011, *Exp. Astron.*, 33, 113
- Axford, W. I., & Hines, C. O. 1961, *Can. J. Phys.*, 39, 1433
- Badman, S. V., Bunce, E. J., Clarke, J. T., Cowley, S. W. H., Gérard, J.-C., Grodent, D., & Milan, S. E. 2005, *J. Geophys. Res.*, 110, 11216
- Bagenal, F. 1992, *Annu. Rev. Earth Planet. Sci.*, 20, 289
- Bagenal, F. 2007, *J. Atmos. Solar-Terr. Phys.*, 69, 387
- Bagenal, F. 2009, in *Comparative Planetary Environments*, ed. C. J. Schrijver & G. L. Siscoe (Cambridge/New York: Cambridge University Press)
- Bagenal, F., & Delamere, P. A. 2011, *J. Geophys. Res.*, 116, 5209
- Bagenal, F., Dowling, T. E., & McKinnon, W. B. 2004, in *Jupiter*, ed. F. Bagenal, T. E. Dowling, & W. B. McKinnon
- Balogh, A. 2010, *Space Sci. Rev.*, 152, 23
- Balogh, A., et al. 2005, *Space Sci. Rev.*, 118, 155
- Barabash, S., et al. 2007, *Nature*, 450, 650
- Belcher, J. W., Lazarus, A. J., McNutt, R. L., Jr., & Gordon, G. S., Jr. 1993, *J. Geophys. Res.*, 98, 15177
- Bell, J. M., Westlake, J., & Waite, J. H., Jr. 2011, *Geophys. Res. Lett.*, 38, 6202
- Bhardwaj, A., & Gladstone, G. R. 2000, *Rev. Geophys.*, 38, 295
- Biermann, L. 1957, *Observatory*, 77, 109
- Bigg, E. K. 1964, *Nature*, 203, 1008

- Bolton, S. J., Thorne, R. M., Bourdarie, S., de Pater, I., & Mauk, B. 2004, in *Jupiter's Inner Radiation Belts*, ed. F. Bagenal, T. E. Dowling, & W. B. McKinnon, 671–688
- Brain, D. A. 2006, *Space Sci. Rev.*, 126, 77
- Brain, D., et al. 2010, *Icarus*, 206, 139
- Breuer, D., Labrosse, S., & Spohn, T. 2010, *Space Sci. Rev.*, 152, 449
- Brice, N. M., & Ioannidis, G. A. 1970, *Icarus*, 13, 173
- Bridge, H. S., et al. 1979, *Science*, 204, 987
- Broadfoot, A. L., et al. 1979, *Science*, 204, 979
- Brown, R. A. 1976, *ApJL*, 206, L179
- Brown, R. A., & Chaffee, F. H., Jr. 1974, *ApJL*, 187, L125
- Bunce, E. J., Cowley, S. W. H., & Yeoman, T. K. 2004, *J. Geophys. Res.*, 109, 9
- Bunce, E. J., et al. 2008, *J. Geophys. Res.*, 113, 9209
- Bunce, E. J., et al. 2010, *J. Geophys. Res.*, 115, 10238
- Cassak, P. A., & Shay, M. A. 2011, *Space Sci. Rev.*, 265
- Chapman, S., & Ferraro, V. C. A. 1930, *Nature*, 126, 129
- Cheng, A. F., Krimigis, S. M., Mauk, B. H., Keath, E. P., & MacLennan, C. G. 1987, *J. Geophys. Res.*, 92, 15315
- Christensen, U. R. 2010, *Space Sci. Rev.*, 152, 565
- Clarke, J. T., et al. 2002, *Nature*, 415, 997
- Clarke, J. T., et al. 2005, *Nature*, 433, 717
- Clarke, J. T., et al. 2009, *J. Geophys. Res.*, 114, 5210
- Connerney, J. E. P. 1981, *J. Geophys. Res.*, 86, 7679
- Connerney, J. E. P. 1993, *J. Geophys. Res.*, 98, 18659
- Connerney, J. 2007, in *Planetary Magnetism*, ed. G. Schubert & T. Spohn (Elsevier)
- Connerney, J. E. P., Acuña, M. H., Ness, N. F., Spohn, T., & Schubert, G. 2004, *Space Sci. Rev.*, 111, 1
- Cowley, S. W. H., & Bunce, E. J. 2001, *Planet. Space Sci.*, 49, 1067
- Cowley, S. W. H., & Bunce, E. J. 2003, *Planet. Space Sci.*, 51, 57
- Cowley, S. W. H., Nichols, J. D., & Bunce, E. J. 2002, *Planet. Space Sci.*, 50, 717
- Cowley, S. W. H., Bunce, E. J., & Nichols, J. D. 2003, *J. Geophys. Res.*, 108, 8002
- Cowley, S. W. H., et al. 2005, *J. Geophys. Res.*, 110, 2201
- Cowley, S. W. H., Nichols, J. D., & Andrews, D. J. 2007, *Ann. Geophys.*, 25, 1433
- Cowley, S. W. H., Badman, S. V., Imber, S. M., & Milan, S. E. 2008a, *Geophys. Res. Lett.*, 35, 10101
- Cowley, S. W. H., et al. 2008b, *Ann. Geophys.*, 26, 2613
- Cowling, T. G. 1933, *MNRAS*, 94, 39
- Crary, F. J., et al. 2005, *Nature*, 433, 720
- Cravens, T. E., Howell, E., Waite, J. H., & Gladstone, G. R. 1995, *J. Geophys. Res.*, 100, 17153
- T. E. Cravens. 1997. *Physics of solar system plasmas*. SAO/NASA Astrophysics Data System. (Cambridge: Cambridge University Press), B529 C72 1997. <http://adsabs.harvard.edu/abs/1997pssp.conf.....C>
- Delamere, P. A. 2009, *J. Geophys. Res.*, 114, 3220
- Delamere, P. A., & Bagenal, F. 2003, *J. Geophys. Res.*, 108, 1276
- Delamere, P. A., & Bagenal, F. 2008, *Geophys. Res. Lett.*, 35, 3107
- Delamere, P. A., & Bagenal, F. 2010, *J. Geophys. Res.*, 115, 10201
- Delamere, P. A., Steffl, A., & Bagenal, F. 2004, *J. Geophys. Res.*, 109, 10216
- Delamere, P. A., Bagenal, F., Dols, V., & Ray, L. C. 2007, *Geophys. Res. Lett.*, 34, 9105
- Delva, M., Mazelle, C., Bertucci, C., Volwerk, M., Vörös, Z., & Zhang, T. L. 2011, *J. Geophys. Res.*, 116, 2318
- Dougherty, M. K., Esposito, L. W., & Krimigis, S. M. 2009, in *Saturn from Cassini-Huygens*, ed. M. K. Dougherty, L. W. Esposito, & S. M. Krimigis
- Dungey, J. W. 1961, *Phys. Rev. Lett.*, 6, 47
- Ergun, R. E., Ray, L., Delamere, P. A., Bagenal, F., Dols, V., & Su, Y.-J. 2009, *J. Geophys. Res.*, 114, 5201
- Finlay, C. C., et al. 2010, *Geophys. J. Int.*, 183, 1216
- Fleshman, B. L., Delamere, P. A., & Bagenal, F. 2010a, *J. Geophys. Res.*, 115, 4007
- Fleshman, B. L., Delamere, P. A., & Bagenal, F. 2010b, *Geophys. Res. Lett.*, 37, 3202
- Galand, M., Moore, L., Mueller-Wodarg, I., Mendillo, M., & Miller, S. 2011, *J. Geophys. Res.*, 116, 9306
- Ge, Y. S., Russell, C. T., & Khurana, K. K. 2010, *Planet. Space Sci.*, 58, 1455
- Gold, T. 1959, *J. Geophys. Res.*, 64, 1219
- Gombosi, T. I. 1998. *Physics of the space environment*. SAO/NASA Astrophysics Data System. (Cambridge/New York: Cambridge University Press) <http://adsabs.harvard.edu/abs/1998pse.conf.....G>
- Grocott, A., Badman, S. V., Cowley, S. W. H., Milan, S. E., Nichols, J. D., & Yeoman, T. K. 2009, *J. Geophys. Res.*, 114, 7219
- Grodent, D., Clarke, J. T., Waite, J. H., Cowley, S. W. H., Gérard, J.-C., & Kim, J. 2003, *J. Geophys. Res.*, 108, 1366
- Grodent, D., Gérard, J.-C., Clarke, J. T., Gladstone, G. R., & Waite, J. H. 2004, *J. Geophys. Res.*, 109, 5201
- Grodent, D., Bonfond, B., Radioti, A., Gérard, J.-C., Jia, X., Nichols, J. D., & Clarke, J. T. 2009, *J. Geophys. Res.*, 114, 7212
- Gurnett, D. A., & Bhattacharjee, A. 2005
- Gurnett, D. A., Persoon, A. M., Kurth, W. S., Groene, J. B., Averkamp, T. F., Dougherty, M. K., & Southwood, D. J. 2007, *Science*, 316, 442

- Gurnett, D. A., Lecacheux, A., Kurth, W. S., Persoon, A. M., Groene, J. B., Lamy, L., Zarka, P., & Carbary, J. F. 2009, *Geophys. Res. Lett.*, 36, 16102
- Gurnett, D. A., Groene, J. B., Persoon, A. M., Menietti, J. D., Ye, S.-Y., Kurth, W. S., MacDowall, R. J., & Lecacheux, A. 2010, *Geophys. Res. Lett.*, 37, 24101
- Hansen, C. J., Esposito, L., Stewart, A. I. F., Colwell, J., Hendrix, A., Pryor, W., Shemansky, D., & West, R. 2006, *Science*, 311, 1422
- Hansen, C. J., et al. 2008, *Nature*, 456, 477
- Hill, T. W. 1979, *J. Geophys. Res.*, 84, 6554
- Hill, T. W., Dessler, A. J., & Maher, L. J. 1981, *J. Geophys. Res.*, 86, 9020
- Hill, T. W., et al. 2008, *J. Geophys. Res.*, 113, 1214
- Huddleston, D. E., Russell, C. T., Kivelson, M. G., Khurana, K. K., & Bennett, L. 1998, *J. Geophys. Res.*, 103, 20075
- Hui, Y., et al. 2010, *J. Geophys. Res.*, 115, 7102
- Hulot, G., Finlay, C. C., Constable, C. G., Olsen, N., & Mandea, M. 2010, *Space Sci. Rev.*, 152, 159
- Jackman, C. M., Achilleos, N., Bunce, E. J., Cecconi, B., Clarke, J. T., Cowley, S. W. H., Kurth, W. S., & Zarka, P. 2005, *J. Geophys. Res.*, 110, 10212
- Jackman, C. M., et al. 2008, *J. Geophys. Res.*, 113, 11213
- Jarvinen, R., Kallio, E., Dyadechkin, S., Janhunen, P., & Sillanpää, I. 2010, *Geophys. Res. Lett.*, 37, 16201
- Jia, X., Walker, R. J., Kivelson, M. G., Khurana, K. K., & Linker, J. A. 2008, *J. Geophys. Res.*, 113, 6212
- Jia, X., Walker, R. J., Kivelson, M. G., Khurana, K. K., & Linker, J. A. 2009, *J. Geophys. Res.*, 114, 9209
- Jia, X., Kivelson, M. G., Khurana, K. K., & Walker, R. J. 2010a, *Space Sci. Rev.*, 152, 271
- Jia, X., Walker, R. J., Kivelson, M. G., Khurana, K. K., & Linker, J. A. 2010b, *J. Geophys. Res.*, 115, 12202
- Johnson, R., Tucker, O., Michael, M., Sitter, E., Smith, H., Young, D., & Waite, J. 2009, Mass loss processes in Titan's upper atmosphere, in *Titan from Cassini-Huygens*, ed. R. H. Brown, J.-P. Lebreton, & J. H. Waite (Dordrecht/New York: Springer)
- Joy, S. P., Kivelson, M. G., Walker, R. J., Khurana, K. K., Russell, C. T., & Ogino, T. 2002, *J. Geophys. Res.*, 107, 1309
- Jurac, S., & Richardson, J. D. 2005, *J. Geophys. Res.*, 110, 9220
- Kanani, S. J., et al. 2010, *J. Geophys. Res.*, 115, 6207
- Khurana, K. K. 2001, *J. Geophys. Res.*, 106, 25999
- Khurana, K. K., & Schwarzl, H. K. 2005, *J. Geophys. Res.*, 110, 7227
- Kivelson, M. G. 2007, Planetary magnetospheres, in *Handbook of the Solar-Terrestrial Environment*, ed. Y. Kamide & A. C.-L. Chian (Berlin/New York: Springer), 470
- Kivelson, M. G., & Russell, C. T. (ed.) 1995
- Kivelson, M. G., & Southwood, D. J. 2005, *J. Geophys. Res.*, 110, 12209
- Kupo, I., Mekler, Y., & Eviatar, A. 1976, *ApJL*, 205, L51
- Kurth, W. S., et al. 2005, *Nature*, 433, 722
- Kurth, W. S., Averkamp, T. F., Gurnett, D. A., Groene, J. B., & Lecacheux, A. 2008, *J. Geophys. Res.*, 113, 5222
- La Belle-Hamer, A. L., Otto, A., & Lee, L. C. 1995, *J. Geophys. Res.*, 100, 11875
- Lamy, L., Cecconi, B., Prangé, R., Zarka, P., Nichols, J. D., & Clarke, J. T. 2009, *J. Geophys. Res.*, 114, 10212
- Lamy, L., et al. 2010, *Geophys. Res. Lett.*, 37, 12104
- Lembege, B., et al. 2004, *Space Sci. Rev.*, 110, 161
- Mauk, B. H., & Fox, N. J. 2010, *J. Geophys. Res.*, 115, 12220
- Mauk, B. H., Krimigis, S. M., Cheng, A. F., & Selesnick, R. S. 1995, in *Neptune and Triton*, ed. D. P. Cruikshank, M. S. Matthews, & A. M. Schumann (Tucson: University of Arizona Press), 169–232
- Mauk, B. H., Anderson, B. J., & Thorne, R. M. 2002, Magnetosphere-ionosphere coupling at Earth, Jupiter, and Beyond, in *Atmospheres in the Solar System: Comparative Aeronomy*, ed. M. Mendillo, A. Nagy, & J. H. Waite (Washington, D.C.: American Geophysical Union), 97
- Mauk, B., et al. 2009, Fundamental plasma processes in Saturn's magnetosphere, in *Saturn from Cassini-Huygens*, ed. S. M. Krimigis, M. K. Dougherty, & L. W. Esposito (Dordrecht/New York: Springer)
- McComas, D. J., & Bagenal, F. 2007, *Geophys. Res. Lett.*, 34, 20106
- McComas, D. J., Allegrini, F., Bagenal, F., Crary, F., Ebert, R. W., Elliott, H., Stern, A., & Valek, P. 2007, *Science*, 318, 217
- McComas, D., et al. 2008, *Space Sci. Rev.*, 140, 261
- McNutt, R. L., Jr., Belcher, J. W., Sullivan, J. D., Bagenal, F., & Bridge, H. S. 1979, *Nature*, 280, 803
- McNutt, R. L., et al. 2007, *Science*, 318, 220
- McNutt, R. L., et al. 2008, *Space Sci. Rev.*, 140, 315
- Merrill, R., McFadden, P., & McElhinny, M. 1996, (*Academic*)
- Moore, T. E., & Horwitz, J. L. 2007, *Rev. Geophys.*, 45, 3002
- Morabito, L. A., Synnott, S. P., Kupferman, P. N., & Collins, S. A. 1979, *Science*, 204, 972
- Nagy, A. F., et al. 2004, *Space Sci. Rev.*, 111, 33
- Ness, N. F. 2010, *Space Sci. Rev.*, 152, 5

- Neubauer, F. M., Gurnett, D. A., Scudder, J. D., & Hartle, R. E. 1984, Titan's magnetospheric interaction, in Saturn ed. T. Gehrels & M. S. Matthews (Tucson: University of Arizona Press), 760–787
- Nichols, J. D., & Cowley, S. W. H. 2005, *Ann. Geophys.*, 23, 799
- Nichols, J. D., et al. 2010, *Geophys. Res. Lett.*, 37, 15102
- Nimmo, F., & Stevenson, D. J. 2000, *J. Geophys. Res.*, 105, 11969
- Olsen, N., Glassmeier, K.-H., & Jia, X. 2010, *Space Sci. Rev.*, 152, 135
- Ozak, N., Schultz, D. R., Cravens, T. E., Kharchenko, V., & Hui, Y.-W. 2010, *J. Geophys. Res.*, 115, 11306
- Pallier, L., & Prangé, R. 2004, *Geophys. Res. Lett.*, 31, 6701
- Parker, E. N. 2007, Conversations on electric and magnetic fields in the cosmos, in *Conversations on Electric and Magnetic Fields in the Cosmos*, ed. E. N. Parker (Princeton: Princeton University Press)
- Paty, C., & Winglee, R. 2006, *Geophys. Res. Lett.*, 33, 10106
- Paty, C., Paterson, W., & Winglee, R. 2008, *J. Geophys. Res.*, 113, 6211
- Peale, S. J., Cassen, P., & Reynolds, R. T. 1979, *Science*, 203, 892
- Phillips, J. L., & Russell, C. T. 1987, *Adv. Space Res.*, 7, 291
- Porco, C. C., et al. 2006, *Science*, 311, 1393
- Radioti, A., Grodent, D., Gérard, J.-C., Bonfond, B., & Clarke, J. T. 2008, *Geophys. Res. Lett.*, 35, 3104
- Radioti, A., Grodent, D., Gérard, J.-C., & Bonfond, B. 2010, *J. Geophys. Res.*, 115, 7214
- Radioti, A., Grodent, D., Gérard, J.-C., Vogt, M. F., Lystrup, M., & Bonfond, B. 2011, *J. Geophys. Res.*, 116, 3221
- Ray, L. C., Su, Y.-J., Ergun, R. E., Delamere, P. A., & Bagenal, F. 2009, *J. Geophys. Res.*, 114, 4214
- Ray, L. C., Ergun, R. E., Delamere, P. A., & Bagenal, F. 2010, *J. Geophys. Res.*, 115, 9211
- Russell, C. T. 1993, *J. Geophys. Res.*, 98, 18681
- Russell, C. T. 2004, *Adv. Space Res.*, 33, 2004
- Russell, C. T. 2006, *Adv. Space Res.*, 37, 1467
- Russell, C. T., & Dougherty, M. K. 2010, *Space Sci. Rev.*, 152, 251
- Russell, C. T., Khurana, K. K., Kivelson, M. G., & Huddleston, D. E. 2000, *Adv. Space Res.*, 26, 1499
- Russell, C. T., Luhmann, J. G., & Strangeway, R. J. 2006, *Planet. Space Sci.*, 54, 1482
- Santos-Costa, D., & Bourdarie, S. A. 2001, *Planet. Space Sci.*, 49, 303
- Saur, J., Schilling, N., Neubauer, F. M., Strobel, D. F., Simon, S., Dougherty, M. K., Russell, C. T., & Pappalardo, R. T. 2008, *Geophys. Res. Lett.*, 35, 20105
- Schneider, N., & Bagenal, F. 2007, Io's neutral clouds, plasma torus and magnetospheric interactions, in *Io After Galileo*, ed. R. M. C. Lopes & J. R. Spencer (Berlin/New York: Springer)
- Schubert, G., Solomatin, V., Tackley, P., & Turcotte, D. 1988, Mantle convection and the thermal evolution of Venus, in *Venus II*, ed. D. Hunten, R. Phillips, & S. W. Bougher (Tucson: University of Arizona Press)
- Scurry, L., & Russell, C. T. 1991, *J. Geophys. Res.*, 96, 9541
- Scurry, L., Russell, C. T., & Gosling, J. T. 1994, *J. Geophys. Res.*, 99, 14811
- Sergis, N., et al. 2010, *Geophys. Res. Lett.*, 37, 2102
- Siscoe, G. L. 1979, Towards a comparative theory of magnetospheres, in *Solar System Plasma Physics*, ed. E. N. Parker, C. F. Kennel, & L. J. Lanzerotti (Amsterdam/New York: North-Holland), 319–402
- Siscoe, G. L., & Summers, D. 1981, *J. Geophys. Res.*, 86, 8471
- Siscoe, G. L., Eviatar, A., Thorne, R. M., Richardson, J. D., Bagenal, F., & Sullivan, J. D. 1981, *J. Geophys. Res.*, 86, 8480
- Sittler, E. C., et al. 2008, *Planet. Space Sci.*, 56, 3
- Sittler, E., Hartle, R., Bertucci, C., Coates, A., Cravens, T., Dandouras, I., & Shemansky, D. 2009, Energy deposition processes in Titan's upper atmosphere and its induced magnetosphere, in *Titan from Cassini-Huygens*, ed. R. H. Brown, J.-P. Lebreton, & J. H. Waite (Dordrecht/New York: Springer)
- Slavin, J. A. 2004, *Adv. Space Res.*, 33, 1859
- Slavin, J. A., & Holzer, R. E. 1979, *J. Geophys. Res.*, 84, 2076
- Slavin, J. A., Smith, E. J., Spreiter, J. R., & Stahara, S. S. 1985, *J. Geophys. Res.*, 90, 6275
- Slavin, J. A., et al. 2007, *Space Sci. Rev.*, 131, 133
- Slavin, J. A., et al. 2009, *Science*, 324, 606
- Slavin, J. A., et al. 2010, *Science*, 329, 665
- Smith, C. G. A. 2011, *MNRAS*, 410, 2315
- Smith, H. T., Johnson, R. E., Perry, M. E., Mitchell, D. G., McNutt, R. L., & Young, D. T. 2010, *J. Geophys. Res.*, 115, 10252
- Smrekar, S., Elkins-Tanton, L., Leitner, J., Lenardic, A., Mackwell, S., Moresi, L., Sotin, C., & Stofan, E. 2007, Tectonic and thermal evolution of Venus and the role of Volatiles, in *AGU Monograph*, Vol. 176, *Exploring Venus as a Terrestrial Planet*, ed. E. R. Stofan, T. E. Cravens, & L. W. Esposito (Washington, DC: American Geophysical Union)

- Southwood, D. 2011, *J. Geophys. Res.*, 116, 1201
- Southwood, D. J., & Kivelson, M. G. 1987, *J. Geophys. Res.*, 92, 109
- Southwood, D. J., & Kivelson, M. G. 2007, *J. Geophys. Res.*, 112, 12222
- Stanley, S., & Bloxham, J. 2006, *Icarus*, 184, 556
- Stanley, S., & Glatzmaier, G. A. 2010, *Space Sci. Rev.*, 152, 617
- Steffl, A. J., Stewart, A. I. F., & Bagenal, F. 2004, *Icarus*, 172, 78
- Steffl, A. J., Delamere, P. A., & Bagenal, F. 2006, *Icarus*, 180, 124
- Steffl, A. J., Delamere, P. A., & Bagenal, F. 2008, *Icarus*, 194, 153
- Stevenson, D. J. 1982, *Geophys. Astrophys. Fluid Dyn.*, 21, 113
- Stevenson, D. J. 2003, *Earth Planet. Sci. Lett.*, 208, 1
- Stevenson, D. J. 2010, *Space Sci. Rev.*, 152, 651
- Stevenson, D. J., Spohn, T., & Schubert, G. 1983, *Icarus*, 54, 466
- Stewart, A. J., Schmidt, M. W., van Westrenen, W., & Liebske, C. 2007, *Science*, 316, 1323
- Swisdak, M., Rogers, B. N., Drake, J. F., & Shay, M. A. 2003, *J. Geophys. Res.*, 108, 1218
- Talboys, D. L., Arridge, C. S., Bunce, E. J., Coates, A. J., Cowley, S. W. H., & Dougherty, M. K. 2009a, *J. Geophys. Res.*, 114, 6220
- Talboys, D. L., Arridge, C. S., Bunce, E. J., Coates, A. J., Cowley, S. W. H., Dougherty, M. K., & Khurana, K. K. 2009b, *Geophys. Res. Lett.*, 36, 19107
- Thomas, N., Bagenal, F., Hill, T. W., & Wilson, J. K. 2004, The Io neutral clouds and plasma torus, in *Jupiter: The Planet, Satellites and Magnetosphere*, ed. F. Bagenal, T. E. Dowling, & W. B. McKinnon (Cambridge, UK/New York: Cambridge University Press), 561–591
- Tokar, R. L., et al. 2009, *Geophys. Res. Lett.*, 36, 13203
- Trafton, L., Parkinson, T., & Macy, W., Jr. 1974, *ApJL*, 190, L85
- Treumann, R. A. 2009, *A&AR*, 17, 409
- van Allen, J. A., & Bagenal, F. 1999, Planetary magnetospheres and the interplanetary medium, in *The New Solar System*, ed. J. K. Beatty, C. Collins Petersen, & A. Chaikin (Cambridge/New York: Cambridge University Press), 39
- Vasyliunas, V. M. 1983, Plasma distribution and flow, in *Physics of the jovian Magnetosphere*, ed. A. J. Dessler (Cambridge: Cambridge University Press), 395–453
- Vasyliūnas, V. M. 2001, *Geophys. Res. Lett.*, 28, 2177
- Vasyliūnas, V. M. 2004, *Adv. Space Res.*, 33, 2113
- Vasyliunas, V. 2009, Fundamentals of planetary magnetospheres, in *Heliophysics: Plasma Physics of the Local Cosmos*, ed. C. J. Schrijver & G. L. Siscoe (Cambridge: Cambridge University Press)
- Vasyliunas, V. 2010, Energy conversion in planetary magnetospheres, in *Heliophysics: Space Storms and Radiation: Causes and Effects*, ed. C. J. Schrijver & G. L. Siscoe (Cambridge: Cambridge University Press), 263
- Vasyliūnas, V. M. 2011, *Space Sci. Rev.*, 158, 91
- Verhille, G., Plihon, N., Bourgoïn, M., Odier, P., & Pinton, J.-F. 2010, *Space Sci. Rev.*, 152, 543
- Vogt, M. F., Kivelson, M. G., Khurana, K. K., Joy, S. P., & Walker, R. J. 2010, *J. Geophys. Res.*, 115, 6219
- Vogt, M. F., Kivelson, M. G., Khurana, K. K., Walker, R. J., Bonfond, B., Grodent, D., & Radioti, A. 2011, *J. Geophys. Res.*, 116, 3220
- Volwerk, M., Delva, M., Futaana, Y., Retinò, A., Vörös, Z., Zhang, T. L., Baumjohann, W., & Barabash, S. 2009, *Ann. Geophys.*, 27, 2321
- Volwerk, M., Delva, M., Futaana, Y., Retinò, A., Vörös, Z., Zhang, T. L., Baumjohann, W., & Barabash, S. 2010, *Ann. Geophys.*, 28, 1877
- Waite, J. H., Jr. et al. 1994, *J. Geophys. Res.*, 99, 14799
- Waite, J. H., et al. 2001, *Nature*, 410, 787
- Waite, J. H., et al. 2006, *Science*, 311, 1419
- Walt, M. 2005, in *Introduction to Geomagnetically Trapped Radiation*, ed. M. Walt (Cambridge/New York: Cambridge University Press)
- Westlake, J. H., Bell, J. M., Waite, J. H., Jr., Johnson, R. E., Luhmann, J. G., Mandt, K. E., Magee, B. A., & Rymer, A. M. 2011, *J. Geophys. Res.*, 116, 3318
- Wicht, J., & Tilgner, A. 2010, *Space Sci. Rev.*, 152, 501
- Woch, J., Krupp, N., & Lagg, A. 2002, *Geophys. Res. Lett.*, 29, 070000
- Young, D. 1997a, Ion and neutral mass spectrometry, in *Encyclopedia of Planetary Sciences*, ed. J. A. Shirley & R. W. Fairbridge (Van Nostrand Reinhold)
- Young, D. 1997b, Space plasma particle instrumentation and the new paradigm: faster, cheaper, better, in *AGU Monograph 102, Measurement Techniques in Space Plasmas: Particles*, ed. D. T. Young, R. F. Pfaff, & J. E. Borovsky (Washington, DC: American Geophysical Union)
- Zarka, P., Lamy, L., Cecconi, B., Prangé, R., & Rucker, H. O. 2007, *Nature*, 450, 265
- Zhang, T. L., et al. 2010, *Geophys. Res. Lett.*, 37, 14202
- Zieger, B., Vogt, J., Glassmeier, K.-H., & Gombosi, T. I. 2004, *J. Geophys. Res.*, 109, 7205